OPTICAL SPECTROSCOPY IN $Li_4Ge_5O_{12}:Mn^{4+}$

AND THE PHOTOREFRACTIVE EFFECT

IN $Bi_{12}SiO_{20}$

By

JIMMY DON ALLEN

Bachelor of Science

Northeastern Oklahoma State University

Tahlequah, Oklahoma

1985

Submitted to the Faculty of the
Graduate College of the
Oklahoma State University
in partial fulfillment of
the requirements for
the Degree of
MASTER OF SCIENCE
December, 1988

OPTICAL SPECTROSCOPY IN $Li_4Ge_5O_{12}:Mn^{4+}$

AND THE PHOTOREFRACTIVE EFFECT

IN $Bi_{12}SiO_{20}$

THESIS APPROVED:

_____
Thesis Advisor

_____

_____

_____
Dean of the Graduate College

ii

ACKNOWLEDGEMENTS

perspective.   Last and foremost I would like to thank my mother and father for the guidance, support and love they have given me in my life.   I owe them far more than I can ever repay, and I dedicate this thesis to Donald B. and Sonja G. Allen, my parents.

TABLE OF CONTENTS

LIST OF TABLES

LIST OF FIGURES

CHAPTER I

INTRODUCTION

Similar spectroscopic techniques were employed to investigate both topics contained in this thesis. The scattering efficiency from a laser-induced grating, which is derived in Chapter II, was utilized in both experiments and proved to be an important parameter.

In Chapter II, the results of investigating $Li_4Ge_5O_{12}:Mn^{4+}$ through a variety of forms of optical spectroscopy, including absorption and fluorescence spectra, time-resolved spectroscopy and fluorescence lifetime studies, are reported. The spectral features are consistent with the presence of two types of sites for the Mn^{4+} ions, and radiationless decay and vibronic transitions are shown to be responsible for the variation of the spectral properties with temperature. Four-wave mixing measurements were performed and the temperature dependence of the four-wave mixing signal is correlated with the temperature dependence of the fluorescence lifetime.

The examination of the photorefractive effect in $Bi_{12}SiO_{20}$ as a function of temperature is related in Chapter III. The band transport model is discussed and useful equations for the photorefractive signal efficiency are

given. The grating buildup and decay are studied for both dark and erasure decay between room temperature and 330°C. Although the time constant follows the predicted behavior at low temperatures, it deviates from the theory at higher temperatures where complex patterns have emerged from the write-decay process. From the results of dark decay measurements it is expected that the temperature dependence of the dark conductivity, σ_d, causes the anomalous behavior at higher temperatures.

Chapter IV describes future work in both materials.

CHAPTER II

OPTICAL SPECTROSCOPY IN $Li_4Ge_5O_{12}$:Mn^{4+}

Introduction

Mn^{4+} has a $3d^3$ electron configuration which is isoelectronic with Cr^{3+}. However, unlike Cr^{3+}, which has extensive amounts of literature describing its optical properties due to its importance in laser applications, Mn^{4+} ions have had very little reported research.[1-5] Thus, they are prime candidates for investigation.

Lithium Germanium Oxide has several possible forms, each with their own chemical formula and crystallographic structure. Crystals of the particular compound studied here were grown by the Czochralski method and found, by x-ray crystallography, to have a triclinic structure with a P_1 space group.[6] In this crystal structure the germanium atoms occupy at least two different types of sites, one with tetrahedral point symmetry and one with octahedral symmetry. The distance between the Ge ions and the oxygen ligands is 1.749 Å in the former type and 1.903 Å in the latter. The ratio of the relative number of these types of sites is 4:6. The Mn^{4+} ions enter the lattice substitutionally for the Ge^{4+} ions. The sample used in this work contained 0.1 at % Mn.

3

It was of irregular shape, approximately 3 mm thick and of yellowish color.

Theory

Four wave mixing (FWM) techniques have been useful in characterizing nonlinear optical properties and exciton dynamics of doped crystals and glasses.[7-10] In these types of experiments, laser-induced population gratings of the metastable states of the dopant ions are established and probed by crossed laser beams tuned to resonance with one of the absorption transitions of the ions. A valuable parameter in this technique is the scattering efficiency, η, which can be derived from a coupled wave theory.

The coupled wave theory of Kogelnik[9] assumes monochromatic light incident at or near the Bragg angle and polarized perpendicular to the plane of incedence of the grating. When the incoming "reference" wave, R, satisfies these requirements, the outgoing "signal" wave, S, is produced. This is illustrated in Figure 1. Wave propogation in the grating is described by the Helmholtz equation:

$$\nabla^2 \vec{E} + k^2 \vec{E} = 0 \tag{1}$$

and the total electric field in the grating is the superposition of the two waves:

$$E = R(z)\exp(i\vec{k_R} \cdot \vec{x}) + S(z)\exp(i\vec{k_S} \cdot \vec{x}) \tag{2}$$

where $R(z)$ and $S(z)$ are the reference and signal beam amplitudes, respectively, and $\vec{k_R}$ and $\vec{k_S}$ are their wave
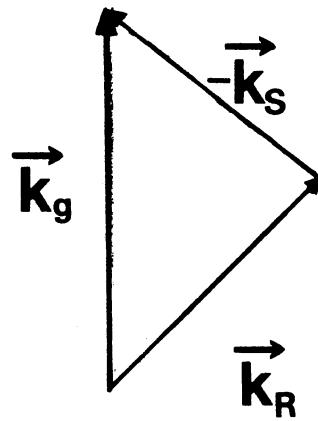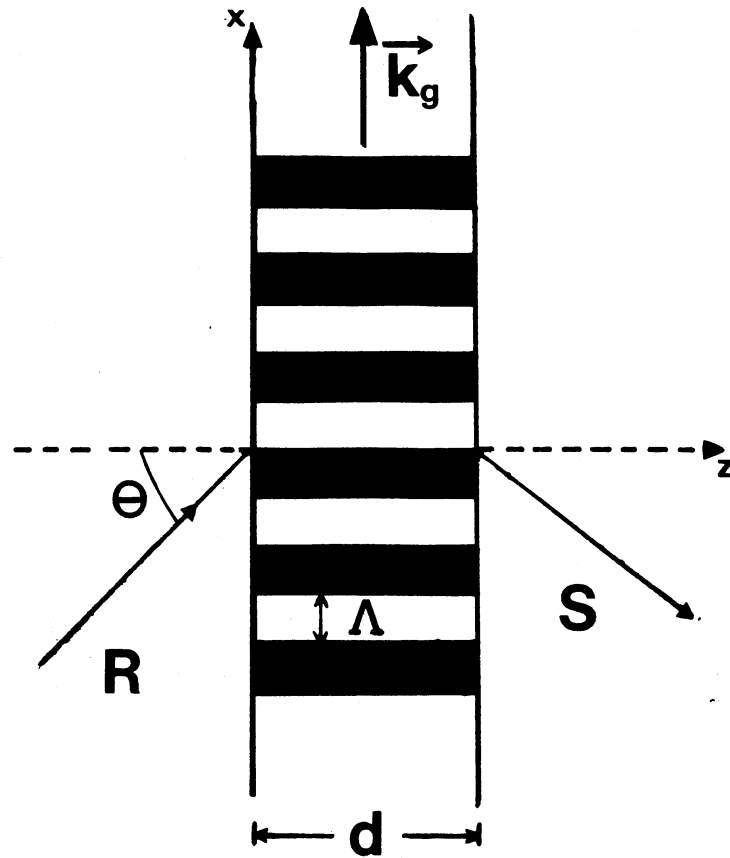
Figure 1. Coupled-wave model for laser-induced gratings.

vectors. The reference and signal beam wave vectors satisfy the Bragg condition

$$\vec{k}_R - \vec{k}_S = \vec{k}_g = k_g\hat{x} \tag{3}$$

where $\vec{k}_g$ is the grating wave vector with a magnitude given by

$$|k_g| = 2\pi/\Lambda \tag{4}$$

where Λ is the grating period.

The behavior of the electric field, $\vec{E}$, in the medium is governed by Maxwell's equations, given here in MKS units.

$$\vec{\nabla} \times \vec{E} = -(\partial\vec{B}/\partial t) \tag{5}$$

$$\vec{\nabla} \times \vec{B} = \mu_m\varepsilon_m(\partial\vec{E}/\partial t) + \mu_m\sigma\vec{E} \tag{6}$$

where μ_m is the permeability, ε_m the permittivity, and σ the conductivity of the medium. The wave equation in the medium may be developed from:

$$\vec{\nabla} \times \vec{E} = -(\partial\vec{B}/\partial t) \tag{5}$$

$$\vec{\nabla} \times (\vec{\nabla} \times \vec{E}) = -\vec{\nabla}\times(\partial\vec{B}/\partial t) \tag{7}$$

$$\vec{\nabla}(\vec{\nabla}\cdot\vec{E})-\nabla^2\vec{E} = -(\partial/\partial t)(\vec{\nabla}\times\vec{B}) \tag{8}$$

$$-\nabla^2\vec{E} = -(\partial/\partial t)[\mu_m\varepsilon_m(\partial\vec{E}/\partial t)+\mu_m\sigma\vec{E}] \tag{9}$$

$$\nabla^2\vec{E} = \mu_m\varepsilon_m(\partial^2\vec{E}/\partial t^2)+\mu_m\sigma(\partial\vec{E}/\partial t). \tag{10}$$

Equation (10) has a plane wave solution given by

$$\vec{E}(x,t) = \vec{E}_0 \exp(i[kx-\omega t]) \tag{11}$$

Substitution of this solution into Equation (10) yields a complex propagation constant

$$k^2 = \mu_m\varepsilon_m\omega^2 + i\omega\mu_m\sigma. \tag{12}$$

If we note that

$$1/v^2 = \mu_m\varepsilon_m = n^2/c^2 \tag{13}$$

where v is the speed of the wave in the medium, n is the index of refraction, and c is the speed of light in free space, then we can write:

$$k^2 = (\omega^2/c^2)n^2 + i\omega\mu_m\sigma \qquad (14)$$

$$k^2 = (\omega^2/c^2)[\mu_m\varepsilon_m/(\mu_0\varepsilon_0)] + i\omega\mu_m\sigma \qquad (15)$$

where μ_0 and ε_0 are the permeability and the permittivity of free space respectively. Since $\mu_m \approx \mu_0 = \mu$ we may write our final expression for the propagation constant,

$$k^2 = (\omega^2/c^2)\varepsilon + i\omega\mu\sigma \qquad (16)$$

where ε is the relative dielectric constant of the medium.

The hologram grating fringes can be represented by a spatial modulation of ε or σ,

$$\varepsilon = \varepsilon_0 + \Delta\varepsilon \cos(k_g x)$$
$$\sigma = \sigma_0 + \Delta\sigma \cos(k_g x) \qquad (17)$$

where $\Delta\varepsilon$ and $\Delta\sigma$ are the amplitudes of spatial modulation while ε_0 and σ_0 are the average dielectric constant and average conductivity, respectively. Combining Equations (16) and (17) yields

$$k^2 = (\omega^2/c^2)\{\varepsilon_0+\Delta\varepsilon\cos(k_g x)\} + i\omega\mu\{\sigma_0+\Delta\sigma\cos(k_g x)\} \qquad (18)$$

$$k^2 = (\omega^2/c^2)\varepsilon_0 + i\omega\mu\sigma_0 + \{(\omega^2/c^2)\Delta\varepsilon\cos(k_g x)$$
$$+ i\omega\mu\Delta\sigma\cos(k_g x)\}. \qquad (19)$$

Utilizing the relation $\omega = 2\pi c/\lambda$, it follows

$$k^2 = (4\pi^2/\lambda^2)\varepsilon_0 + i(2\pi c/\lambda)\mu\sigma_0 + \{(4\pi^2/\lambda^2)\Delta\varepsilon\cos(k_g x) +$$
$$i(2\pi c/\lambda)\mu\Delta\sigma\cos(k_g x)\} \qquad (20)$$

which may be written as

$$k^2 = \beta^2 + 2i\beta\alpha + 4\kappa\beta\cos(k_g x) \qquad (21)$$

with the definitions

$$\beta = \text{average propagation constant} = (2\pi/\lambda)\varepsilon_0^{\frac{1}{2}} \qquad (22)$$

$$\alpha = \text{average absorption coefficient} = c\mu\sigma_0/(2\varepsilon_0^{\frac{1}{2}}) \qquad (23)$$

$$\kappa = \text{coupling constant} = \frac{1}{4}[(2\pi/\{\lambda\varepsilon_0^{\frac{1}{2}}\})\Delta\varepsilon + i(\mu c/\varepsilon_0^{\frac{1}{2}})\Delta\sigma]. \quad (24)$$

The coupling constant, κ, describes the coupling between the reference wave, R, and the signal wave, S. It is the central parameter in the coupled wave theory since, if κ is zero, there is no coupling and, therefore, no diffraction.

The propagation constant, k, may be written as

$$k = (\omega/c)\{\varepsilon + i(c^2\mu/\omega)\sigma\}^{\frac{1}{2}}. \qquad (25)$$

In free space the propagation constant would simply be k = ω/c, so we may consider the wave travelling in the medium to be modified by the complex index of refraction n[11]

$$n = n_R + in_I = \{\varepsilon + i(c^2\mu/\omega)\sigma\}^{\frac{1}{2}}. \qquad (26)$$

Using a binomial expansion for n, we may write

$$n_R + in_I \approx \varepsilon^{\frac{1}{2}} + i(c^2\mu\sigma/[2\omega\varepsilon^{\frac{1}{2}}]) \qquad (27)$$

neglecting higher order terms. If we assume that $n_R \gg n_I$, which is valid in most practical cases, then we may write

$$n_0 \approx n_R = \varepsilon^{\frac{1}{2}} \approx \varepsilon_0^{\frac{1}{2}} \qquad (28)$$

and

$$\Delta n \approx \Delta\varepsilon/(2\varepsilon_0^{\frac{1}{2}}) \qquad (29)$$

where n_0 is the average and Δn the spatial modulation of the index of refraction. Similarly, for the spatial modulation of the absorption coefficient the results are

$$\alpha_0 = \mu c\sigma_0/(2\varepsilon_0^{\frac{1}{2}}) \qquad (30)$$

and

$$\Delta\alpha = \mu c\Delta\sigma/(2\varepsilon_0^{\frac{1}{2}}). \tag{31}$$

Substituting these values into Equation (24) yields an expression for the coupling constant

$$\kappa = \text{coupling constant} = \frac{1}{4}[(2\pi/\{\lambda\varepsilon_0^{\frac{1}{2}}\})\Delta\varepsilon + i(\mu c/\varepsilon_0^{\frac{1}{2}})\Delta\sigma] \tag{24}$$

$$\kappa = (\pi/\{2\lambda\varepsilon_0^{\frac{1}{2}}\})\Delta\varepsilon + i(\mu c/\{4\varepsilon_0^{\frac{1}{2}}\})\Delta\sigma \tag{32}$$

$$\kappa = (\pi/\lambda)\Delta n + (i/2)\Delta\alpha. \tag{33}$$

Combining Equations (1) and (21), we may write

$$\nabla^2\vec{E} + \{\beta^2 + 2i\beta\alpha + 4\kappa\beta\cos(k_g x)\}\vec{E} = 0. \tag{34}$$

If we assume that energy interchange between R and S is slow and that energy absorption is negligible, we may neglect second order derivatives. We may also neglect waves generated in the $(\vec{k}_g + \vec{k}_R)$ and $(\vec{k}_g - \vec{k}_S)$ directions along with higher order diffraction terms. Inserting Equations (2) and (3) into Equation (34) along with the previous assumptions allows us to write:

$$\nabla^2\vec{E} + \{\beta^2 + 2i\beta\alpha + 4\kappa\beta\cos(k_g x)\}\vec{E}$$

$$= \{2ik_R R' + 2i\alpha\beta R + 2\kappa\beta S\} \exp(ik_R x)$$

$$+ \{2ik_S S' + 2i\alpha\beta S + 2\kappa\beta R\} \exp(ik_S x) = 0. \tag{35}$$

Each bracketed term must be equal to zero for this to occur.

$$2ik_R R' + 2i\alpha\beta R + 2\kappa\beta S = 0 \tag{36}$$

$$2ik_S S' + 2i\alpha\beta S + 2\kappa\beta R = 0 \tag{37}$$

Multiplication of both equations by the quantity $(i/2\beta)$ yields

$$C_R R' + \alpha R = i\kappa S \tag{38}$$

$$C_S S' + \alpha S = i\kappa R \tag{39}$$

where $C_R = C_S = \cos\theta$. The physical picture of the
diffraction process is seen in the coupled wave equations
(38) and (39). A wave changes in amplitude due to coupling
to the other wave (κS, κR) or absorption (αS, αR). To solve
the coupled wave equations, general solutions of the form

$$R(z) = r_1 \exp(\gamma_1 z) + r_2 \exp(\gamma_2 z) \tag{40}$$

$$S(z) = s_1 \exp(\gamma_1 z) + s_2 \exp(\gamma_2 z) \tag{41}$$

are substituted into (38) and (39) and the γ's are solved
for. This yields

$$(C_R \gamma_j + \alpha) r_j = i\kappa s_j \tag{42}$$

$$(C_S \gamma_j + \alpha) s_j = i\kappa r_j \tag{43}$$

Multiplication of these equations by one another gives a
quadratic equation for γ_j

$$C_R C_S \gamma_j^2 + \alpha(C_R + C_S)\gamma_j + (\alpha^2 + \kappa^2) = 0 \tag{44}$$

which has solutions

$$\gamma_{1,2} = -(\alpha/\cos\theta) \pm i(\kappa/\cos\theta). \tag{45}$$

For a transmission hologram the boundary conditions are

$$R(0) = 1; \quad S(0) = 0 \tag{46}$$

Inserting these conditions into the general solutions,
Equations (40) and (41), yields

$$r_1 + r_2 = 1$$

and $\tag{47}$

$$s_1 + s_2 = 0$$

Combining these relations with Equation (43) we obtain

$$s_1 = -s_2 = i\kappa/\{C_S(\gamma_1 - \gamma_2)\}. \tag{48}$$

output of the grating

$$S(d) = s_1[\exp(\gamma_1 d) - \exp(\gamma_2 d)]. \qquad (49)$$

Using Equation (45) this may be rewritten as

$$S(d) = \tfrac{1}{2}\exp(-\alpha d/\cos\theta) [\exp(i\kappa d/\cos\theta) - \exp(-i\kappa d/\cos\theta)] \quad (50)$$

The fraction of the incident light power which is diffracted into the signal wave is called the scattering efficiency, η , which is given by

$$\eta = SS^*. \qquad (51)$$

Using the expression for κ from Equation (33) the scattering efficiency reduces to

$$\eta = \exp(-2\alpha d/\cos\theta) [\sin^2(\{\pi d/\lambda\cos\theta\}\Delta n)$$
$$+ \sinh^2(\{d/2\cos\theta\}\Delta\alpha)] \qquad (52)$$

which is the experimentally determinable scattering efficiency.

Experiment

Equipment and Procedure

The absorption spectra of $Li_4Ge_5O_{12}:Mn^{4+}$ were recorded on a Perkin-Elmer model 330 spectrophotometer. Fluorescence spectra were obtained using a Spex 1-m monochromator, an RCA C31034 photomultiplier tube, an EG&G/PAR lock-in amplifier, and a strip chart recorder. The exitation was provided by the 488-nm line of a Spectra Physics argon laser. For fluorescence lifetime measurements, a Molectron nitrogen laser was used to provide excitation pulses 10ns in duration at 333.7-nm and the signals were processed with either an EG&G/PAR boxcar averager or signal averager. The sample was

EG&G/PAR boxcar averager or signal averager. The sample was mounted in a cryogenic refrigerator capable of controlling the temperatures between 12 K and room temperature.

The experimental four-wave mixing (FWM) setup is shown in Figure 2. The gratings were written with the 488-nm line of a Spectra Physics argon laser. The laser output was split with a beam splitter into two beams of equal power (write beams) which travel equal path lengths before crossing at an angle θ inside the sample. A He-Ne laser was used to read the gratings. For measuring the FWM signal efficiency the laser beams were chopped and lock-in detection was used to improve the signal-to-noise ratio. The signal decay kinetics were measured with a signal averager.

Results

Absorption. The absorption spectrum of $Li_4Ge_5O_{12}$:Mn^{4+} at 12 K is shown in Figure 3. The presence of Mn^{4+} ions introduces a broad band peaked near 420-nm which is probably associated with transitions from the $^4A_{2g}$ ground state to the $^4T_{2g}$ level. As the temperature was raised to 300 K this band changed very little. The absorption edge of the material near 300-nm was also altered by the Mn^{4+} presence. This is probably associated with transitions from the ground state to the $^4T_{1g}$ level. This band also remained fairly steady as the temperature was raised. No sharp lines were seen even at 12 K.
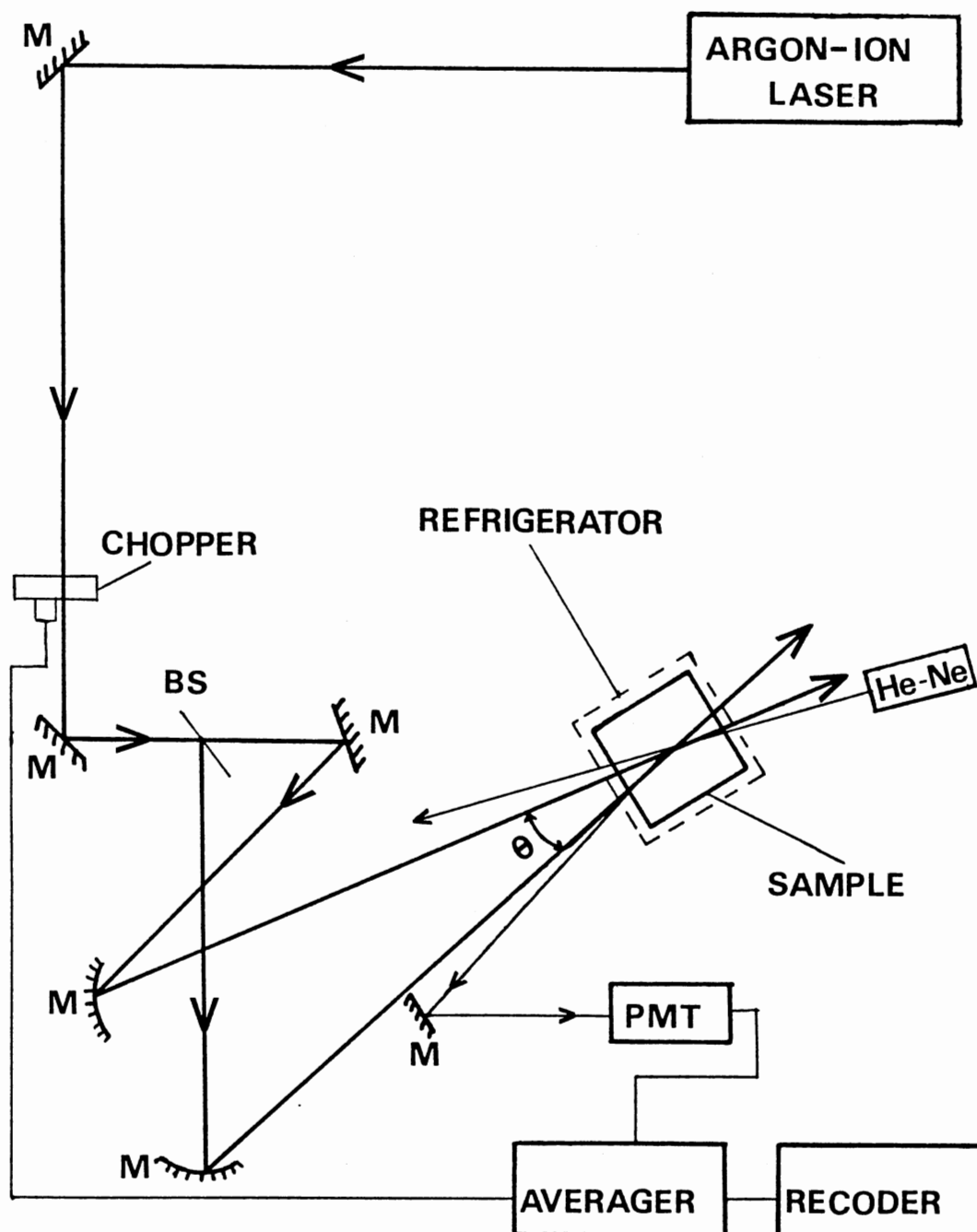
Figure 2. Block diagram of the experimental FWM setup.
BS – Beam splitter; M – Mirror
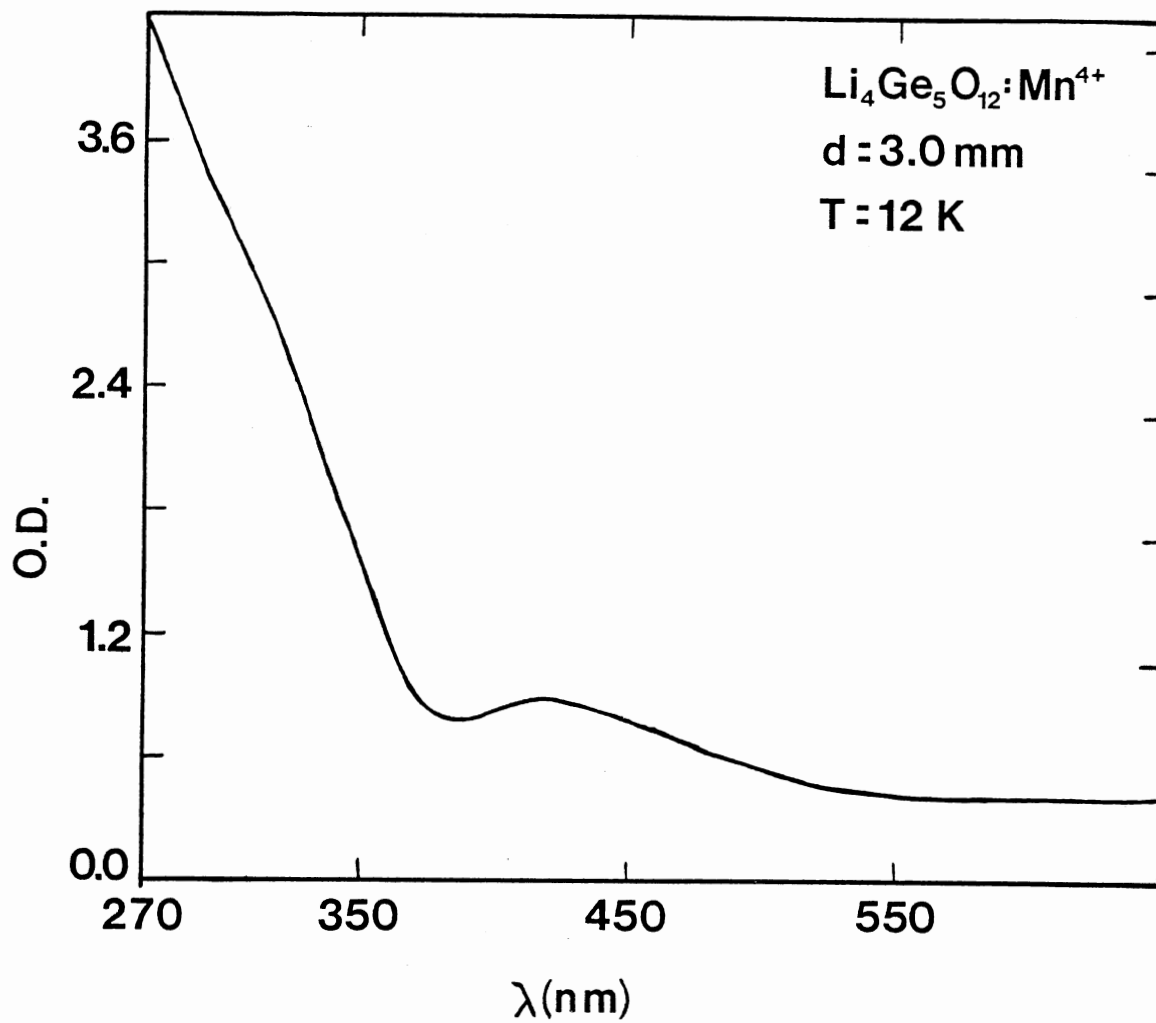
Figure 3. Absorption spectrum of $Li_4Ge_5O_{12}:Mn^{4+}$ crystal
at 12 K

Fluorescence. Figure 4 shows the fluorescence spectrum
at 12 K obtained by exciting the $^4T_{2g}$ absorption band with
the 488-nm line. The spectrum consists of two very intense,
sharp lines and a weak, broad band at lower energies. These
characteristics are typical for a $3d^3$ ion in a relatively
strong crystal field environment, and thus the standard
designations of R_1 and R_2 are used for the two components of
the ^2E_g level to the ground state. Figure 5 shows an
expanded view of the spectra in the regions near both R
lines for two different temperatures. Both R_1 and R_2 are
split into two components labeled R_1^a, R_1^b and R_2^a, R_2^b
respectively. The splitting is 2.55 cm^{-1} for R_1 and 2.04 cm^{-1}
for R_2.

Computer fits were generated for the curves in Figure 5
utilizing a least squares technique.[12] Lorentzian
lineshapes were found to fit the curves with a much higher
degree of accuracy than Gaussian lineshapes, and the best
fits obtained using the Lorentzian lineshapes with variable
intensities, full width at half maximum, $\Delta\lambda$, and peak
positions are shown as the broken lines in Figure 5. The
ratio of the total intensities of the low energy to the high
energy components are plotted as a function of temperature
in Figure 6. The ratios are approximately constant up to
about 70 K and then increase significantly for both lines.
As the temperature increases the individual components of
the lines broaden and become difficult to separate. Above

Figure 4. Fluorescence spectrum of $Li_4Ge_5O_{12}:Mn^{4+}$ crystal at 12 K
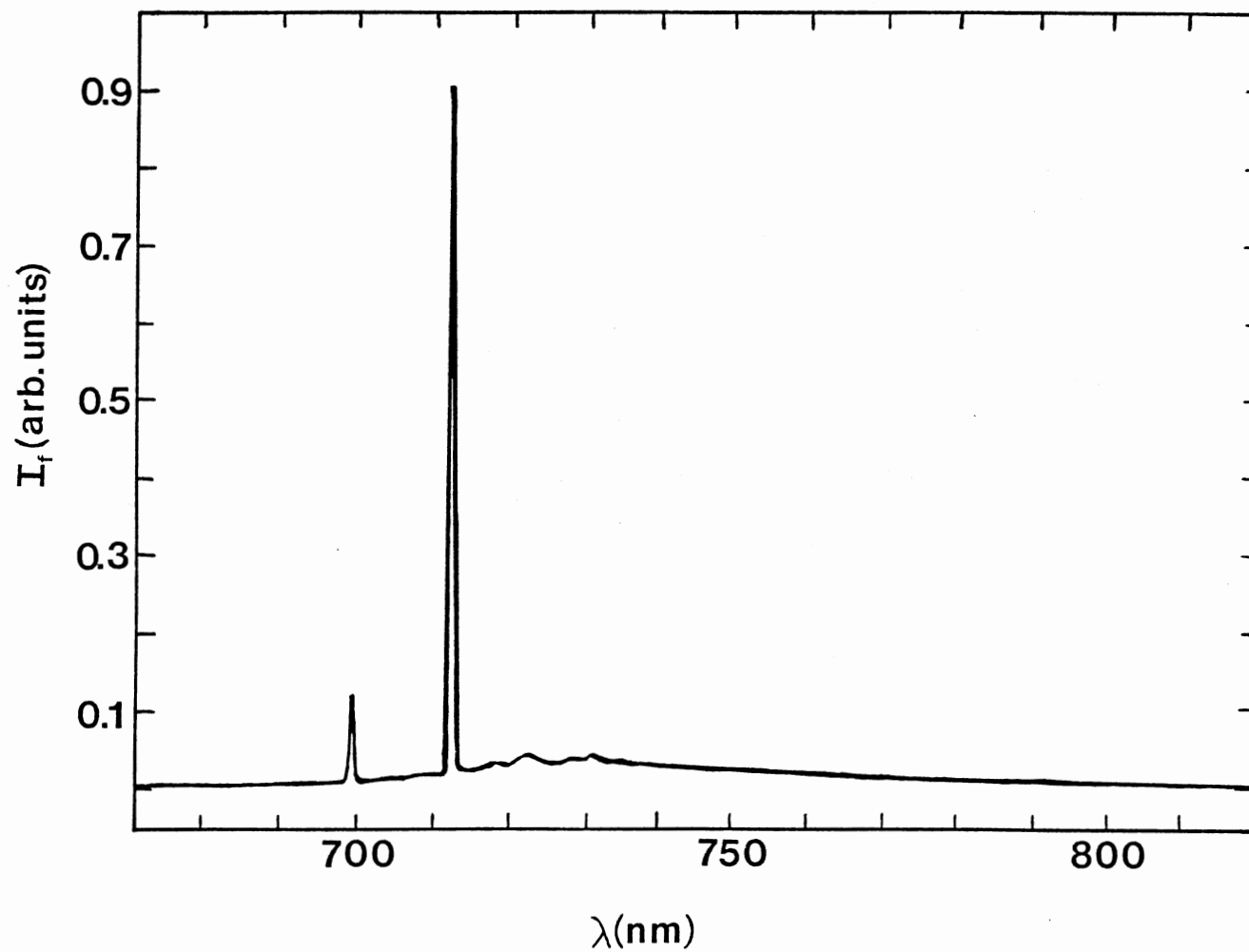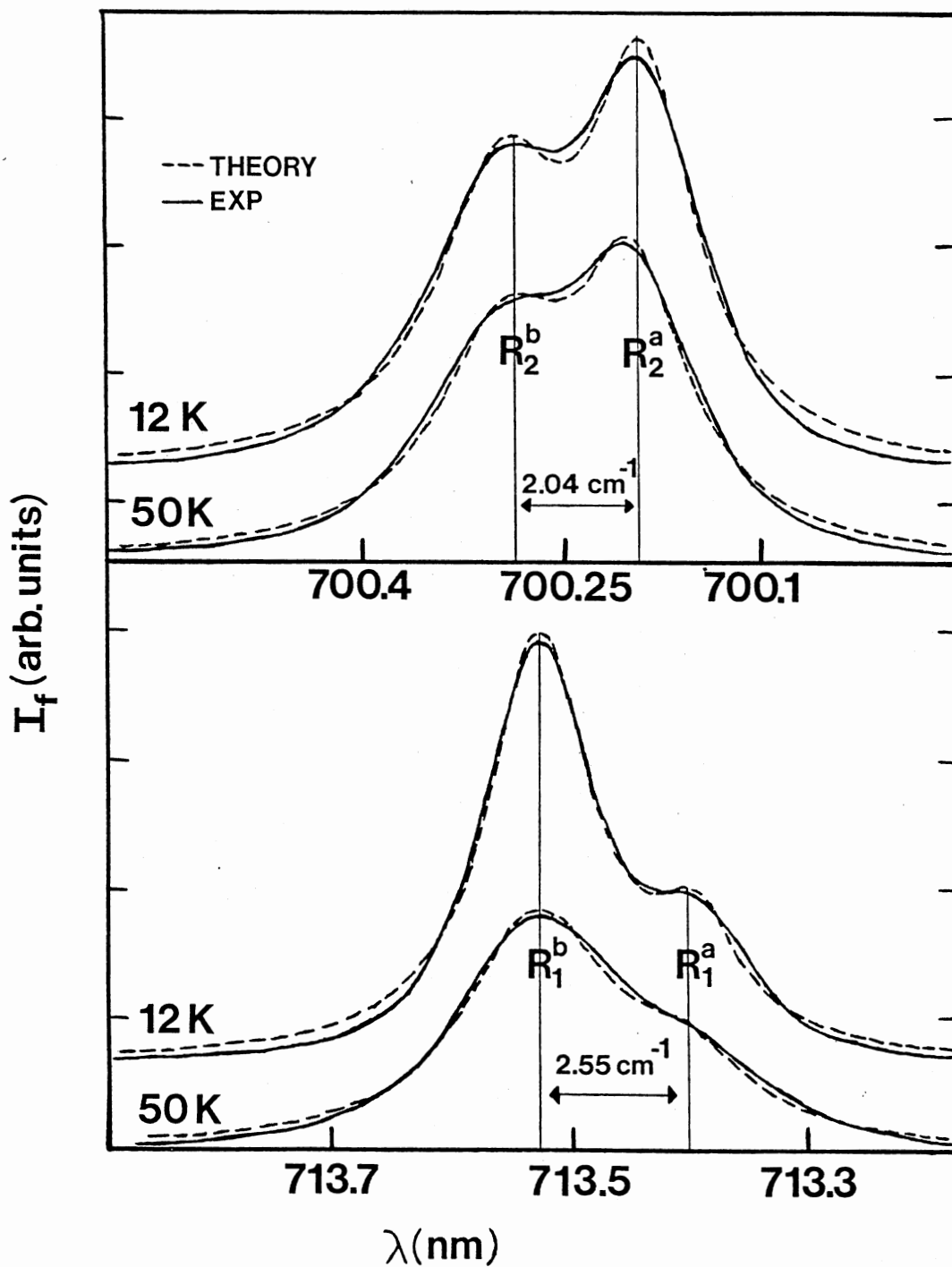
Figure 5. Fluorescence spectrum in the region of the R
lines (solid lines) and the theoretical fits
of Lorentzian curves (broken lines).
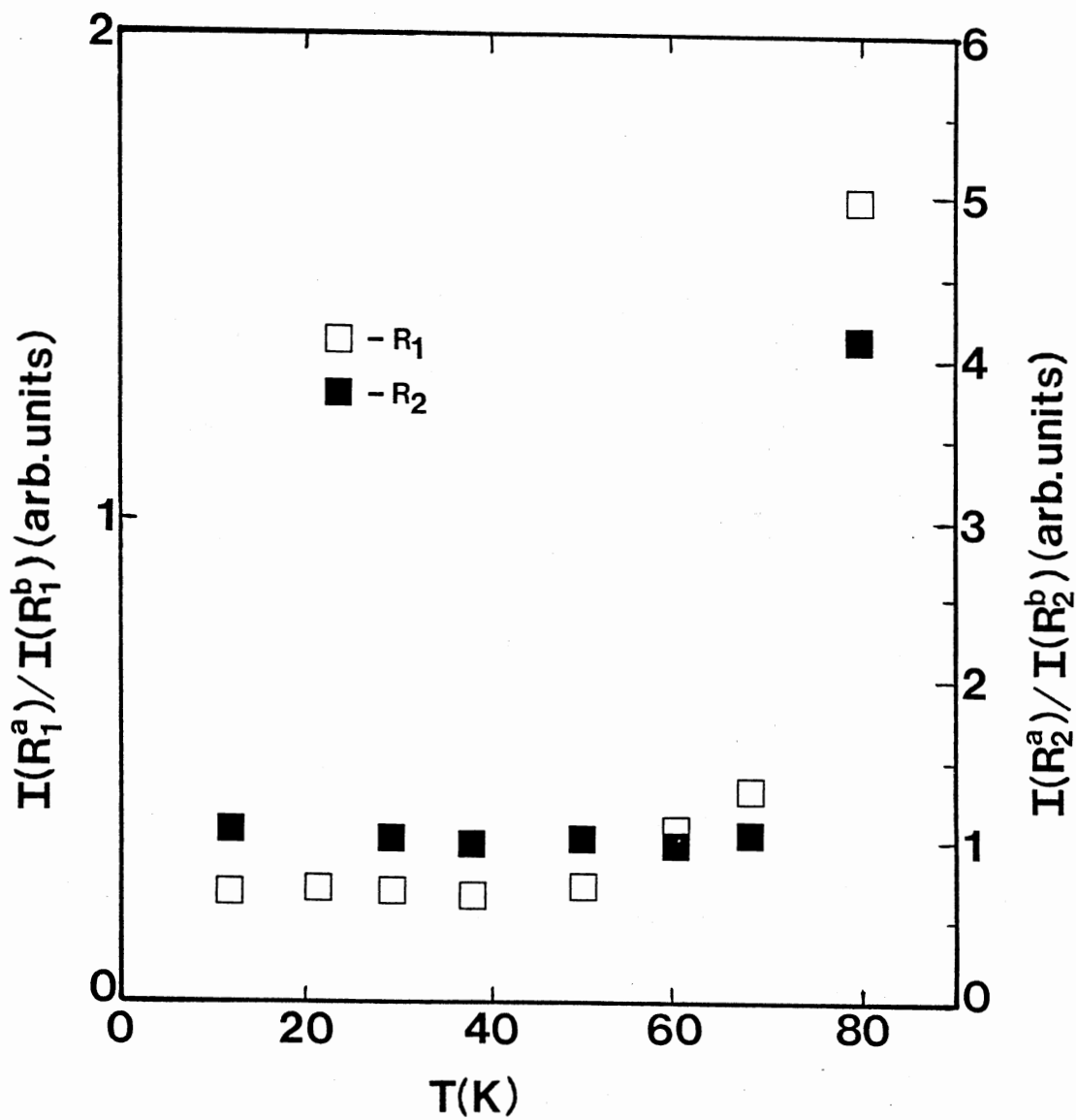
Figure 6. Temperature dependence of the relative total
intensities of the two sets of R lines

100 K they have broadened to the extent that they cannot be resolved.

The lower energy broad band is the vibronic sideband of the zero-phonon R lines. The vibronic sideband is shown in greater detail in Figure 7. The position of the vibronic peaks with respect to the R_1 and R_2 lines are listed in Table 1.

The temperature dependence of the fluorescence intensity at the peak of the vibronic emission band is shown in Figure 8. The intensity is constant from 12 K to about 40 K. From 40 K to around 90 K it decreases to approximately 20 % of its initial valve. This decrease can be described by an expontial with an activation energy of 360 cm^{-1}. The intensity then increases slightly between 90K and 180 K, which is probably associated with an increase in the vibronic transition probability. Above 180 K there is a strong quenching of the fluorescence which is probably associated with an increase in the radiationless decay probability. The fluorescence decay profiles were monitored at the maximum of the vibronic sideband for various temperature and examples are shown in Figure 9. Below 80 K the decay kinetics can be described by doubly exponential functions. Below 40 K the fast component has a characteristic decay time of about 260 μs. At higher temperatures this decreases and the decay curves become single exponentials with the longer decay component remaining above 80 K. The longer component has a decay time
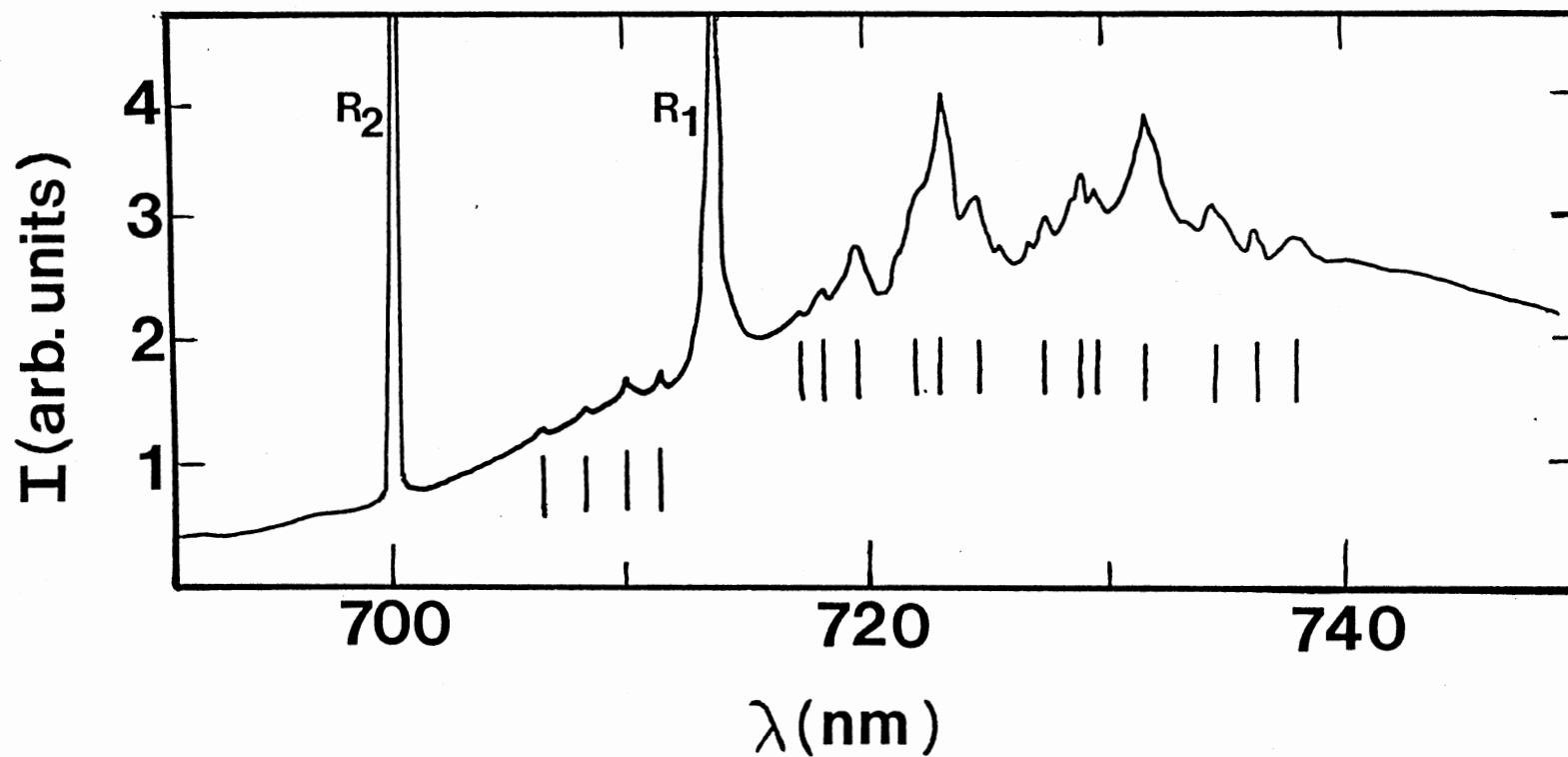
Figure 7. Vibronic emission band of $Li_4Ge_5O_{12}:Mn^{4+}$ at 12 K with the main vibronic peaks marked by vertical lines

TABLE I

VIBRONIC EMISSION PEAKS IN THE FLUORESCENCE

SPECTRUM OF $Li_4Ge_5O_{12}:Mn^{4+}$

λ (nm)	ν (cm^{-1})	$\Delta\nu-R_2$ (cm^{-1})	$\Delta\nu-R_1$ (cm^{-1})
706.4	14156	126	
708.1	14122	160	
709.8	14088	195	
711.2	14061	222	
715.4	13979		37
718.2	13924		92
719.7	13895		121
722.2	13847		168
723.7	13818		198
724.9	13795		220
727.6	13744		272
729.1	13716		300
729.8	13702		313
731.9	13663		352
734.7	13611		404
736.5	13578		438
738.2	13546		469

Figure 8. Temperature dependence of the peak fluorescence intensity.
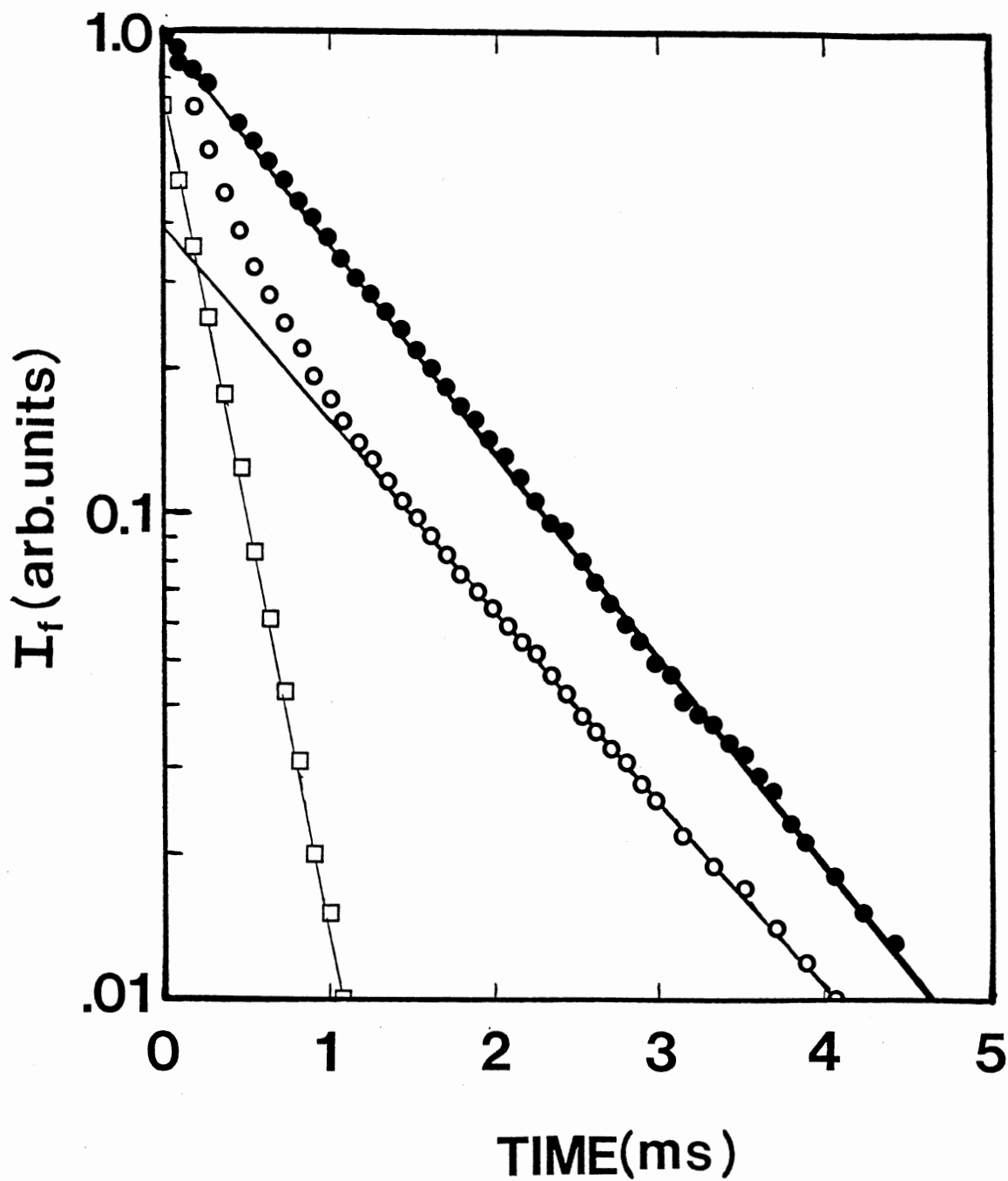
Figure 9. Fluorescence decay kinetics of $Li_4Ge_5O_{12}:Mn^{4+}$ at 138.4 K (full circles) and 35.2 K (open circles). The open squares represent the initial decay at 35.2 K after subtraction of the longer decay component.

of approximately 1.06 ms which remains constant up to 150 K
and then decreases. The temperature dependences of these
decay times are shown in Figure 10 as τ_L (long) and τ_S
(short). These spectral characteristics are summarized in
Table II.

The temperature dependence of the fluorescence decay
rate of ions in site "a", τ^{-1}, can be described as the sum
of the contributions from vibronic and nonradiative
transitions

$$\tau^{-1} = \tau^{-1}_{vib} + \tau^{-1}_{non}. \tag{53}$$

The vibronic contribution can be represented by an
average phonon frequency <w>. This leads to a temperature
dependence for the vibronic contribution of

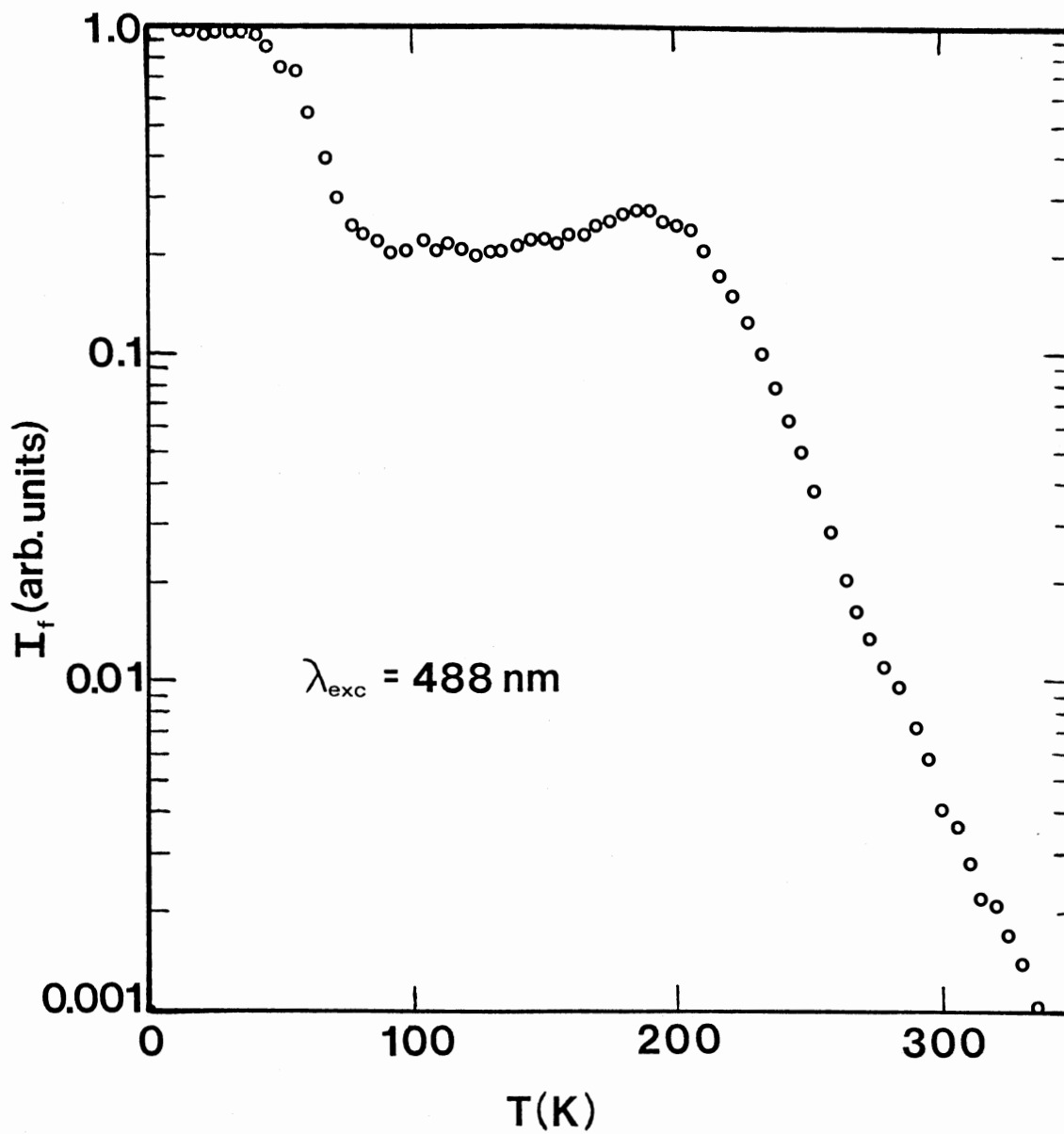$$\tau^{-1}_{vib} = \tau^{-1}_{vib}(o)\coth(<\hbar\omega>/\{2kT\}) \tag{54}$$

where k is the Boltzmann constant and T is the temperature.

The fluorescence decay time may be thermally quenched
by several types of nonradiative transitions. Typically for
Cr^{3+} ions in relatively weak crystal field sites the
nonradiative contribution to the fluorescence lifetime is
associated with the thermal population of the $^4T_2$ level. In
the case of this sample, however, the energy gap between the
^2E and the $^4T_2$ levels is too large for this process to
contribute significantly to the fluorescence lifetime in the
temperature range of interest. The type of nonradiative
transition which appears to be more important in this case
is the direct decay process between the ^2E level and ground
state. This occurs through the emission of p phonons each
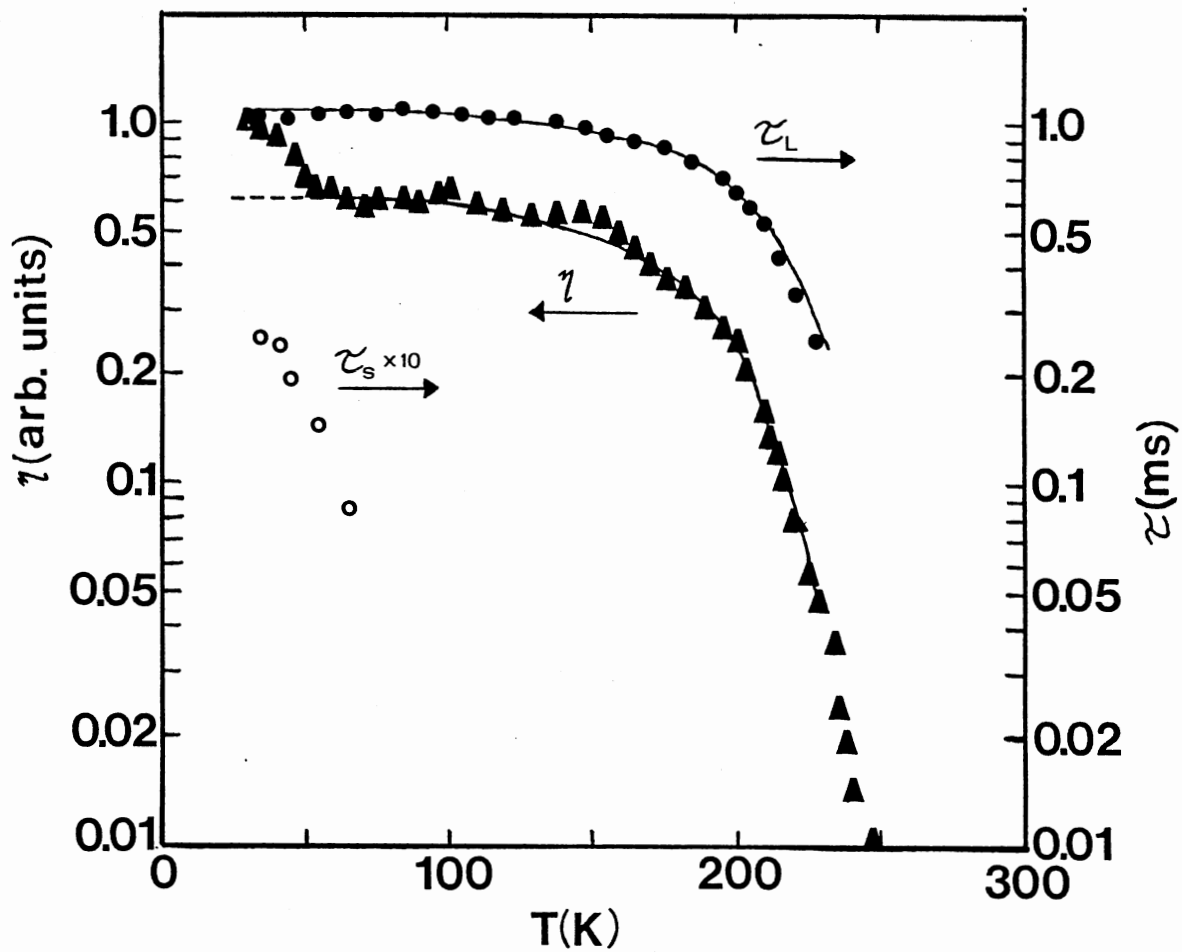
Figure 10. Temperature dependences of the short (open
circles) and long (full circles) components
of the fluorescence lifetimes, and of the
FWM scattering efficiency. The solid lines
represent theoretical fits to the data

TABLE II

SPECTROSCOPIC PROPERTIES OF Mn^{4+} IN

$Li_4Ge_5O_{12}$ CRYSTALS

Parameter	Site a	Site b
R_1 line (nm)	713.40	713.53
R_2 line (nm)	700.19	700.29
$\Delta\lambda$ for R_1 at 12 K (Å)	0.84	1.04
$\Delta\lambda$ for R_2 at 12 K (Å)	0.97	1.25
Splitting of the ^2E level (cm^{-1})	264.50	265.00
τ at 12 K (ms)	1.08	0.26
Quenching temperature (K)	180	40

having an effective energy of $\hbar\omega$, where $p\hbar\omega$ is the energy gap crossed by the transition. The temperature dependence of this contribution to the fluorescence decay rate is[4,13]

$$\tau^{-1}_{non}(T) = RI_p(2s\{n[n+1]\}^{\frac{1}{2}})[(n+1)/n]^{p/2}\exp(-s[1+2n]) \quad (55)$$

where

$$n = [\exp(\{\hbar\omega/kT\}-1)]^{-1} \quad (56)$$

is the phonon occupation number, s is the Huang-Rhys parameter, $I_p(x)$ is a modified Bessel function and R is a temperature-independent prefactor.

The solid line in Figure 10 represents the best fit to the data obtained from Equations (53)-(56) treating the parameters describing the electron-phonon coupling as adjustable parameters. The good fit between theory and experiment shown in the figure is obtained using $\hbar\omega = 325$ cm^{-1}, $\tau_{vib}(o) = 924$s^{-1}, $s = 0.2$, $p = 43$ and $R = 4.89$ x 10^{83} s^{-1}. These results are consistent with those in Reference 4 for Mn^{4+} in $Y_3Al_5O_{12}$.

Four-Wave Mixing. The temperature dependence of the scattering efficiency is shown in Figure 10. Like the fluorescence intensity it initially decreases, then remains constant to about 150 K and then rapidly decreases above this temperature. The decay kinetics of the FWM signals were found to be described by double exponentials at 42 K and single exponentials at 210 K. Figure 11 shows the variation of the signal decay rate on the crossing angle of the write beams. For both temperatures the FWM signal decay
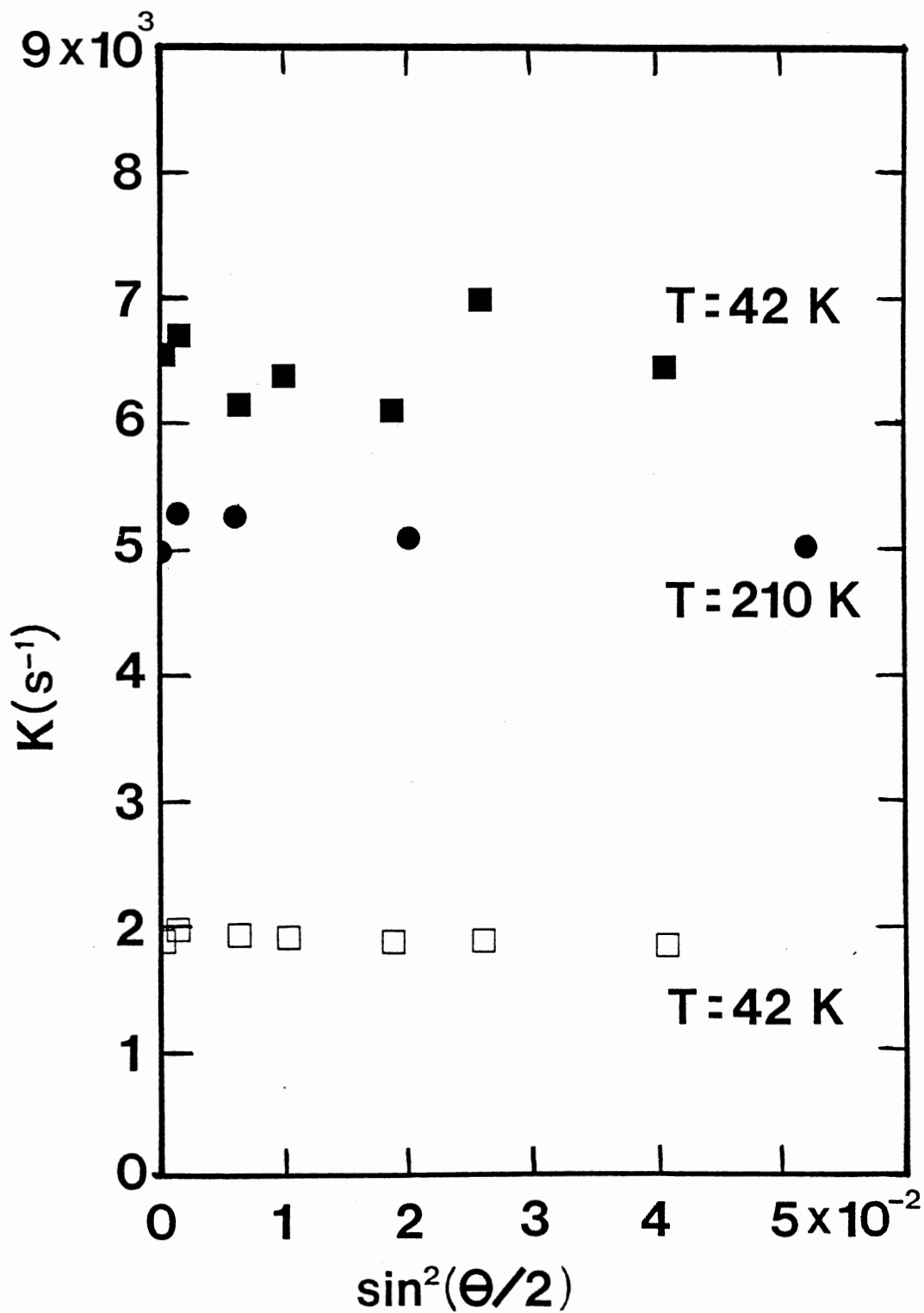
Figure 11. FWM grating decay rate for T = 210 K (circles)
and for 42 K (short component – full squares :
long component – open squares)

rates are independent of crossing angles and are approximately equal to twice the fluorescence decay rates.

The characteristics of the FWM signal are consistent with scattering from a population grating of excited Mn^{4+} ions. At low temperatures the doubly exponential behavior can be attributed to establishing population gratings independently in the two subsets of manganese ions in nonequivalent crystal field sites having different fluorescence lifetimes. The lack of dependence of the grating decay rates on the crossing angle of the write beams indicates that there is no long range energy diffusion in this material. Time resolved spectroscopy measurements were also performed on this material selectively exciting either site "a" or site "b" transitions. The time evolution of the fluorescence emission after selective excitation shows that no energy transfer takes place between ions in different types of sites. Thus, the temperature dependence of the intensity ratios shown in Fig. 6 is due to differences in radiationless quenching and not site-to-site energy transfer.

The theoretical expression for the FWM signal previously derived is given by Equation (52)

$$\eta = \exp(-2\alpha d/\cos\theta) \ [\sin^2(\{\pi d/\lambda\cos\theta\}\Delta n)$$
$$+ \sinh^2(\{d/2\cos\theta\}\Delta\alpha)]. \tag{52}$$

The first term represents the contribution to the signal due to a dispersion grating of modulation depth Δn, and the second term represents the contribution due to an

absorption grating of modulation depth $\Delta\alpha$. For population gratings, the modulation depths can be expressed in terms of products of the concentration of ions in the peak regions of the gratings N_{2p}, with the differences in either the absorption or dispersion of the ions in the ground and excited states. Using the rate equations describing the dynamics of a simple two-level system,[14]

$$N_{2p} = 2I_0 N_0 \sigma_1 / [2I_0 \sigma_1 + (h\nu/\tau)] \tag{57}$$

where I_0 is the intensity of the laser pump beam, N_0 is the total concentration of active ions, σ_1 is the absorption cross section for ions in level 1, $h\nu$ is the photon energy, and τ is the fluorescence lifetime of the metastable state. The parameter that dominates the temperature dependence of the four-wave mixing signal for population gratings is the fluorescence lifetime. For weak gratings, the functions in Equation (52) can be expanded and the signal expressed as

$$\eta = C[1/(A + B/\tau)]^2 \tag{58}$$

where the temperature independent constants A, B and C have different meanings for absorption gratings and dispersion gratings.

Equation (58) can be used to relate the temperature dependences of the fluorescence lifetimes and the four-wave mixing signal intensity. At temperatures below 80 K, the four-wave mixing signal has contributions due to scattering from Mn^{4+} ions in both types of crystal fields sites, as indicated by the double exponential kinetics of the signal. Fluorescence quenching occurs for the ions in one type of

site above 40 K, resulting in a decrease in the scattering efficiency. Above 80 K the FWM signal is due to scattering only from Mn^{4+} in the other type of site. Using the measured values of the fluorescence lifetimes in Equation (58) and treating A, B and C as adjustable constants results in the solid line fitting the FWM data shown in Figure 10. This good fit confirms the relationship between the FWM signal and the metastable state lifetime for a population grating. Not enough independent information is available to interpret the values of the adjustable constants in terms of the contributions to the grating modulation depths and thicknesses.

Four-wave mixing measurements on several other host crystals doped with Cr^{3+}, which is again isoelectronic with Mn^{4+}, have shown that dispersion gratings make the dominant contribution to the scattering efficiency.[8,10,14-17] However, for this case, Figure 3 shows a significant difference in absorption strength for light at the laser wavelength for ions in the ground and excited metastable state, and thus the possibility of a strong contribution from an absorption grating cannot be ruled out.

Discussion and Conclusions

The spectroscopic properties of Mn^{4+} in $Li_4Ge_5O_{12}$ crystals can be explained by assuming that the Mn^{4+} ions occupy two nonequivalent types of crystal field sites. The observed doublet structure of the R lines cannot be

associated with the ground state splitting of an ion in a single type of site since the magnitude of the splitting is different for the R_1 and R_2 lines. The ions in one type of site produce the transitions labeled R_1^a and R_2^a which have the 1.06 ms lifetime at low temperatures. The fluorescence of this center undergoes radiationless quenching above 180 K. The ions in the other type of site produce the transitions labeled R_1^b and R_2^b which have the 260 μs lifetime at low temperature. The fluorescence of this center undergoes radiationless quenching above about 40 K. From the optical data alone, it is not possible to identify the exact nature of the two types of sites. However, it is reasonable to expect that they are the two types of Ge^{4+} sites in this crystal lattice structure.

CHAPTER III

THE PHOTOREFRACTIVE EFFECT

IN $Bi_{12}SiO_{20}$

Introduction

The photorefractive effect (PRE) is the term used to describe the light induced refractive index change in photoconductive electro-optic materials. There has been a significant amount of interest in characterizing the PRE in sillenite-type crystals such as $Bi_{12}SiO_{20}$ (BSO) and $Bi_{12}GeO_{20}$ (BGO) due to their excellent suitability for holographic storage. Some of the recent work describes various aspects of the dynamic response of these crystals during the writing and erasure of photorefractive gratings under different experimental conditions.[18-29] Although the dependence of the photorefractive response of BSO on an applied electric field has been well characterized, little work has been done in determining the variation of the photorefractive response with temperature.

This section of the thesis reports the investigation of the PRE dynamics in BSO using 442-nm light. The signal response shape, writing time, and rate of dark and erasure decay were recorded as a function of temperature with no

applied electric field. The band transport model was then
applied to the signal response at all times.

Theory

The band transport model[23] of the PRE assumes that
photoexcited electrons (or holes) are ejected from filled
donor (or acceptor) sites to the conduction (or valence)
band. Here they migrate to dark regions in the crystals by
drift or diffusion before recombining into empty donors (or
acceptors). The charge separation results in a space charge
field which modulates the refractive index through the
linear electro-optic effect. For simplicity we will deal
only with photoexcited electrons, in which case the band
transport model is described by:

a)   A continuity equation for the mobile conduction band
      electrons:

$$\partial n/\partial t = G - R + (1/e)\ \vec{\nabla}\cdot\vec{J} \qquad (59)$$

where n is the free electron number density, t is time,
G and R are the rate at which free electrons are
created and destroyed, respectively, e is the electron
charge and $\vec{J}$ is the electron current density. The
electron current density is assumed to be the sum of a
diffusion component and a drift component

$$\vec{J} = eD\vec{\nabla}n + q\mu n\vec{E} \qquad (60)$$

where D is the diffusion coefficient, μ is the mobility
and $\vec{E}$ is the electric field. Some materials require

another term added to Equation (60) to take account of the bulk photovoltaic effect; however, this term is negligible in BSO.

b)   A continuity equation for immobile ionized donors:

$$\partial N_D^+ / \partial t = G - R \tag{61}$$

where N_D^+ is the ionized donor density. The generation rate is linearly proportional to the number of occupied donors and the probability rate of ionization.

$$G = (N_D - N_D^+)(sI + \beta) \tag{62}$$

where N_D is the total density of donors, s is the photoexcitation constant, I is the light intensity and β is the probability of thermal excitation. Similarly the recombination rate is linearly proportional to the number of free electrons and the probability that a trap is empty.

$$R = \gamma_R N_D^+ n \tag{63}$$

where γ_R is the recombination constant.

c)   Gauss's Law:

$$\vec{\nabla} \cdot (\varepsilon \vec{E}) = e(N_D^+ - N_A - n) \tag{64}$$

where ε is the static permitivity and N_A is the number of acceptors.

d)   The electro-static condition:

$$\vec{\nabla} \times \vec{E} = 0 \tag{65}$$

which is simply one of Maxwell's equations in the quasi-steady approximation ($\partial \vec{B} / \partial t \approx 0$)

In summary, we may write the band transport equations:

$$\partial N_D^+ / \partial t = (N_D - N_D^+)(sI + \beta) - \gamma_R N_D^+ n \tag{66}$$

$$\partial n/\partial t = \partial N_D^+/\partial t + \nabla \cdot (D\nabla n + \mu n E) \qquad (67)$$

$$\vec{\nabla} \cdot \varepsilon\vec{E} = e(N_D^+ - N_A - n) \qquad (68)$$

The equations are nonlinearly coupled, but can be solved if we assume a quasi-steady approximation in the zeroth-order number density, n_0, linearization in the grating modulation index, m, and cosinusoidal illumination given by[23,30,32]

$$I = I_0\{1 + m\cos(k_g z)\} \qquad (69)$$

where m is the modulation index, k_g is the grating wavevector and I_0 is the average irradiance. With these approximations and omitting those terms that are important only for high irradiance (Mw/cm^2) nanosecond pulses,[34] we obtain the space charge field δE as given by Kukhtarev:[30]

$$\delta E = mE_{SC}[-\cos(k_g z + \psi) + \exp(-t/\tau)\cos(k_g z + \omega t + \psi)] \qquad (70)$$

where E_{SC} is the space charge field amplitude, ω is the transient response frequency and ψ is the phase shift between I and δE in the steady state. The transient response has an overdamped oscillatory behavior with a response time.

$$\tau = \tau_{di} \frac{(1 + \tau_R/\tau_D)^2 + (\tau_R/\tau_E)^2}{[1 + \tau_R\tau_{di}/(\tau_D\tau_I)](1 + \tau_R/\tau_D) + (\tau_R/\tau_E)^2(\tau_{di}/\tau_I)} \qquad .(71)$$

with,

$$\tau_{di} = \varepsilon/(4\pi e\mu n_0) \text{ (dielectric relaxation time)} \qquad (72)$$

$$\tau_E = 1/(k_g\mu E_0) \text{ (drift time)} \qquad (73)$$

$$\tau_D = e/(\mu k_B T k_g^2) \text{ (diffusion time)} \qquad (74)$$

$$\tau_R = 1/(\gamma_R N_A) \text{ (recombination time)} \qquad (75)$$

$$\tau_I = 1/(sI_0 + \gamma_R n_0) \text{ (inverse of sum of photoproduction and ion recombination rates)} \qquad (76)$$

where T is the temperature, and the zeroth-order electron number density is given by

$$n_0 = sI_0(N_D - N_A)/(\gamma_R N_A).$$

(77)

We also need an electro-optic relation between the space charge field and the change in the crystal refractive index given by:[23]

$$\Delta n = \tfrac{1}{2}n_b^3 r_{eff}\delta E$$

(78)

where n_b is the background refractive index and r_{eff} is the effective electro-optic coefficient.

We may then write for the change in the refractive index:

$$\Delta n = \tfrac{1}{2}n_b^3 r_{eff}\ m\ E_{sc}[-\cos(k_g z+\psi)$$
$$+ \exp(-t/\tau)\cos(k_g z+\omega t+\psi)].$$

(79)

Recalling the Kogelnik expression for the diffraction efficiency, Equation (52), we may write for a refractive index grating;

$$\eta = \exp(-2\alpha d/\cos\theta)\sin^2(\pi d\Delta n/\{\lambda\cos\theta\}).$$

(80)

substituting the expression for Δn from Equation (73)

$$\eta = \exp(-2\alpha d/\cos\theta)\sin^2(\pi dn_b^3 r_{eff}mE_{sc}/\{2\lambda\cos\theta\}[-\cos(k_g z+\psi)$$
$$+ \exp(-t/\tau)\cos(k_g z+\omega t+\psi)]).$$

(81)

After some algebra and a trigonometric identity, the diffraction efficiency may be written as:

$$\eta = A\ \sin^2(B[\exp(-t/\tau)\cos(\omega t)-1]-C\exp(-t/\tau)\sin(\omega t))$$

(82)

during writing, with the designations

$$A = \exp(-2\alpha d/\cos\theta)$$

$$B = [\pi dn_b^3 r_{eff}mEsc/\{2\lambda\cos\theta\}]\cos(k_g z+\psi)$$

$$C = [\pi dn_b^3 r_{eff}mEsc/\{2\lambda\cos\theta\}]\sin(k_g z+\psi).$$

The analogous expression during decay is given by:

$$\eta = A \sin^2(\exp(-t/\tau) \ [B \cos(\omega t) + C \sin(\omega t)]) \qquad (83)$$

Experiment

Equipment and Procedure

A block diagram of the experimental setup used for this work is shown in Figure 12. The sample was an oriented crystal of BSO obtained from Crystal Technology. The sample thickness was about 3.9 mm parallel to the <110> crystallographic direction.

A He-Cd laser at 442-nm was used to produce laser induced refractive index gratings (primary holograms) in the sample. The laser output was split into two beams which were expanded and crossed inside the sample. This produced uniform illumination of the entire sample. The crossing angle of the beams outside the sample was $12°$ and the grating wave vector was oriented in a <110> direction. This is referred to as the perpendicular sample orientation ($\perp$ <001>) which gives the optimum diffraction efficiency.[35,36]

The intensities of the two write beams were nearly equal so that $m \approx 1$.

An electro-mechanical shutter was used to shut off the write beams and allow the writing-decay cycle to be repeated several times. For erasure decay measurements, one of the beams was cut off by the shutter while the other beam was left on to erase the grating. For dark decay measurements, both write beams were cut off by the shutter.
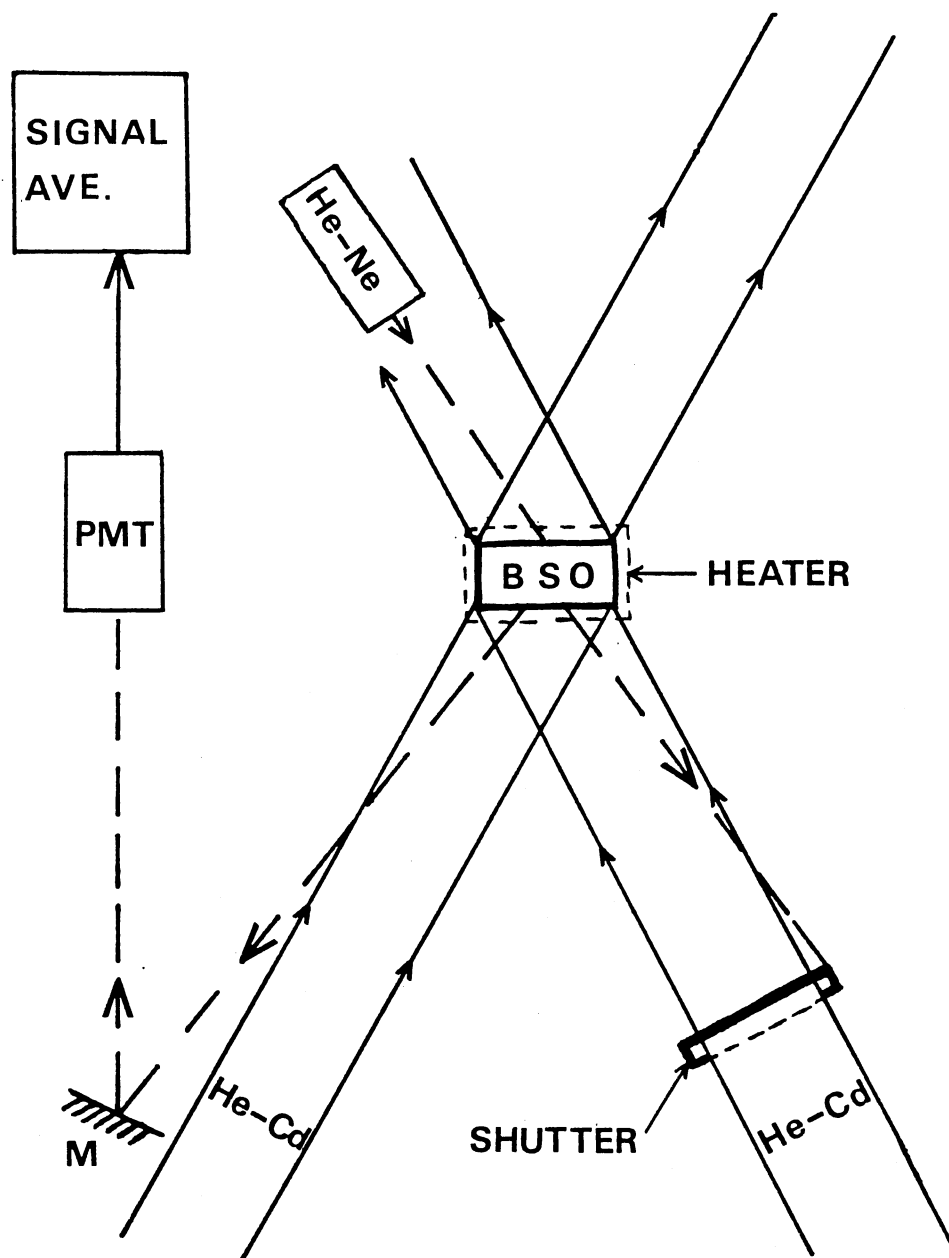
Figure 12. Block diagram of the experimental setup. He-Cd
refers to the helium-cadmium laser; and PMT is
the photomultiplier tube. The results are sent
from a signal averager to a chart recorder

The probe beam was provided by a He-Ne laser incident at the Bragg angle to the grating formed by the write beams. Part of the probe beam was diffracted by the grating and detected as the signal beam by an RCA C31034 photomultiplier tube. By using a red probe beam (633-nm) with a low intensity (<3mW/cm^2) the grating was left undisturbed by the reading process.[24,25,36] The signal was averaged over a large number of cycles by an EG&G/PAR signal averager and recorded on a strip chart recorder.

The sample was mounted in a holder with a cartridge heater and a chromel-alumel thermocouple allowing the temperature to be controlled up to 350°C. No electric field was applied to the sample so that charge transport occurs only through carrier diffusion.

The absorption spectrum was recorded on a Perkin-Elmer model 330 spectrophotometer, and is shown in Fig. 13. The He-Cd excitation is well within the heavily absorbing region and the He-Ne is well removed from it.

Results and Discussions

The time evolution of the photorefractive signal efficiency during both dark and erasure decay is shown in Figures 14 (a - j) for several temperatures. At temperatures up to 157°C the buildup and decay patterns are approximately exponential in behavior except for a slight deviation near steady-state conditions associated with beam depletion within the sample. Above 157°C anomalous patterns
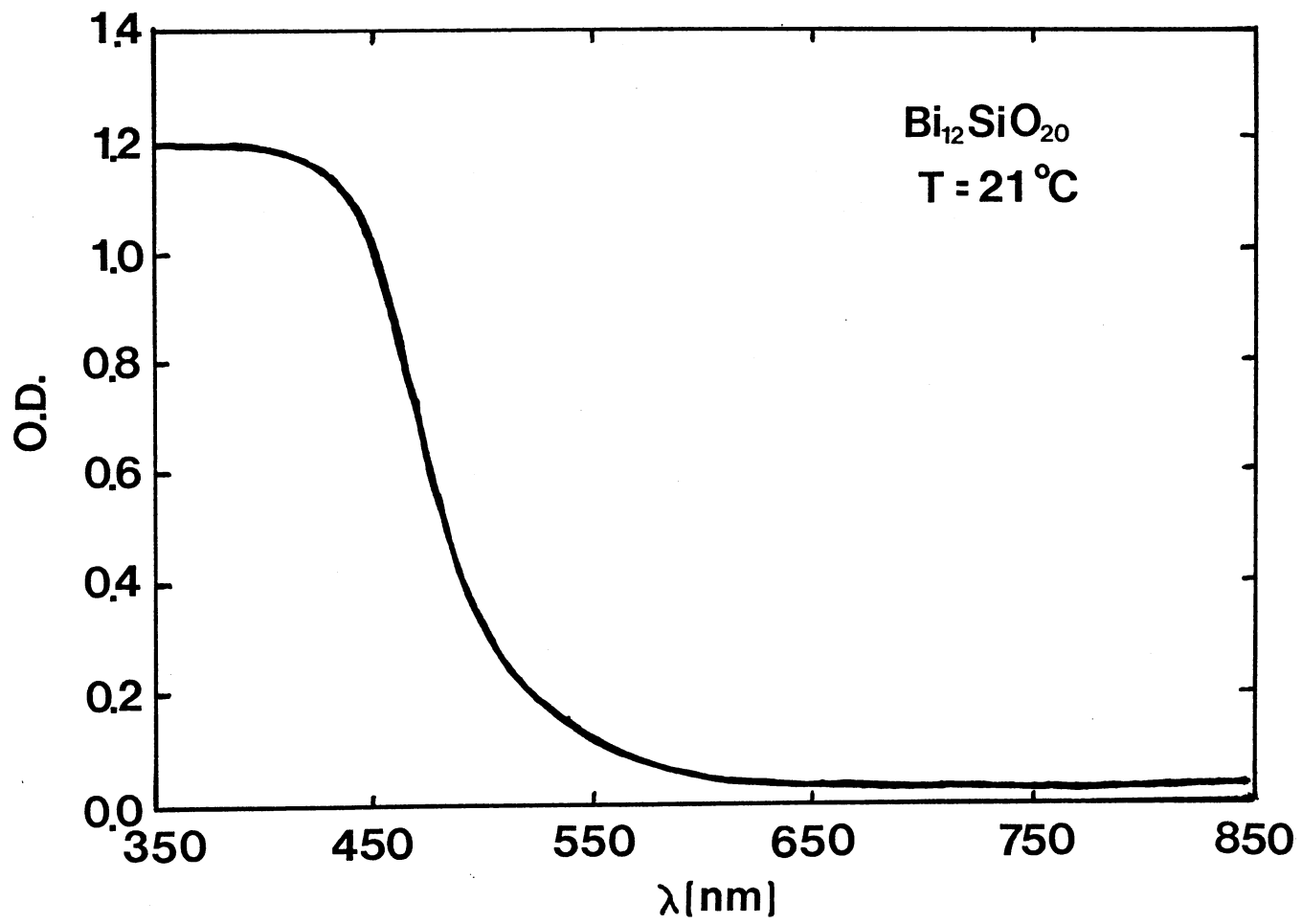
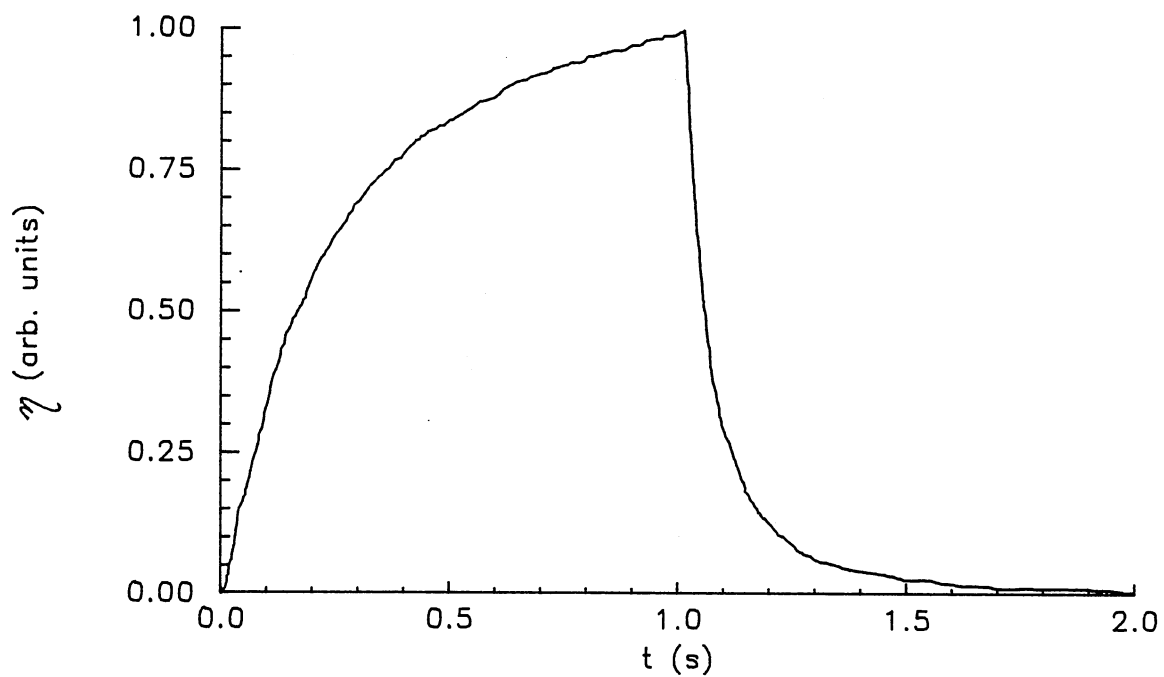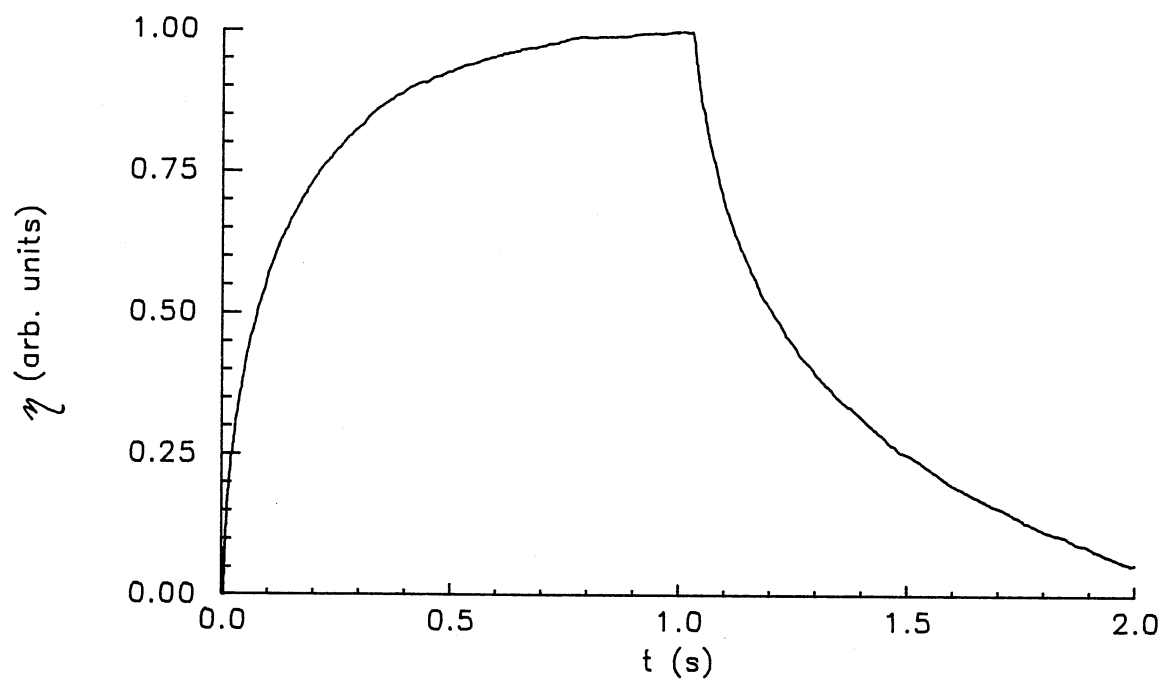Figure 13. Absorption spectrum of $Bi_{12}SiO_{20}$ crystal at room temperature

Figure 14. Time evolution of the signal patterns for
writing and decay of holographic gratings
in BSO; (a) dark decay at 21°C and (b)
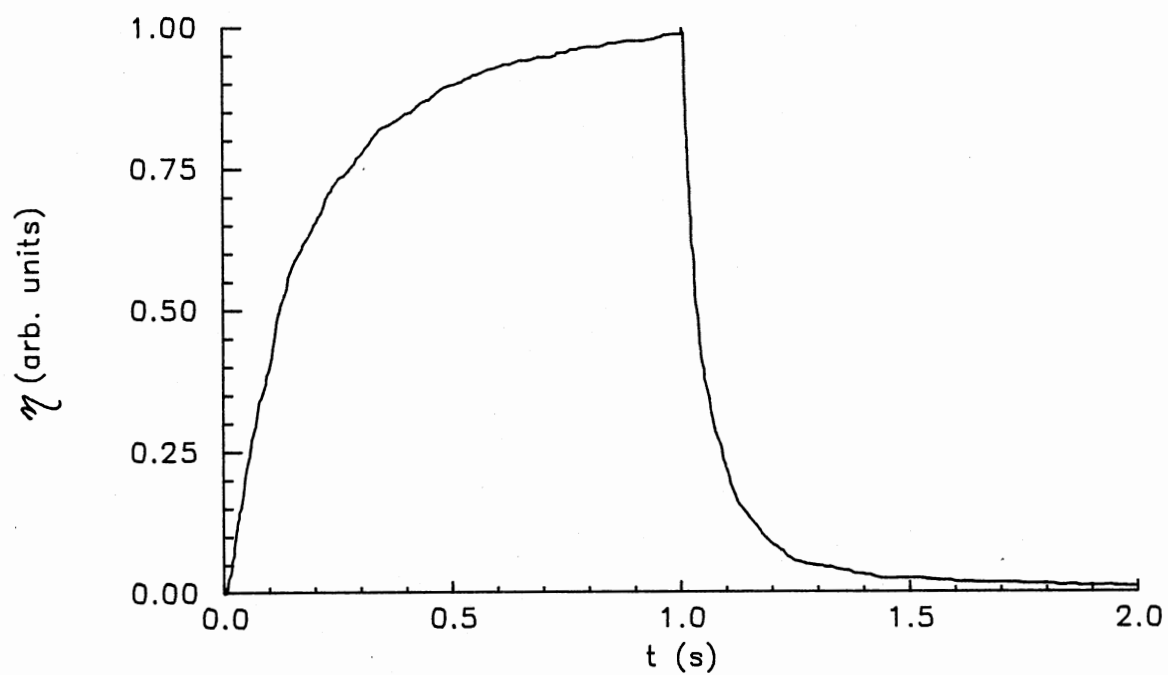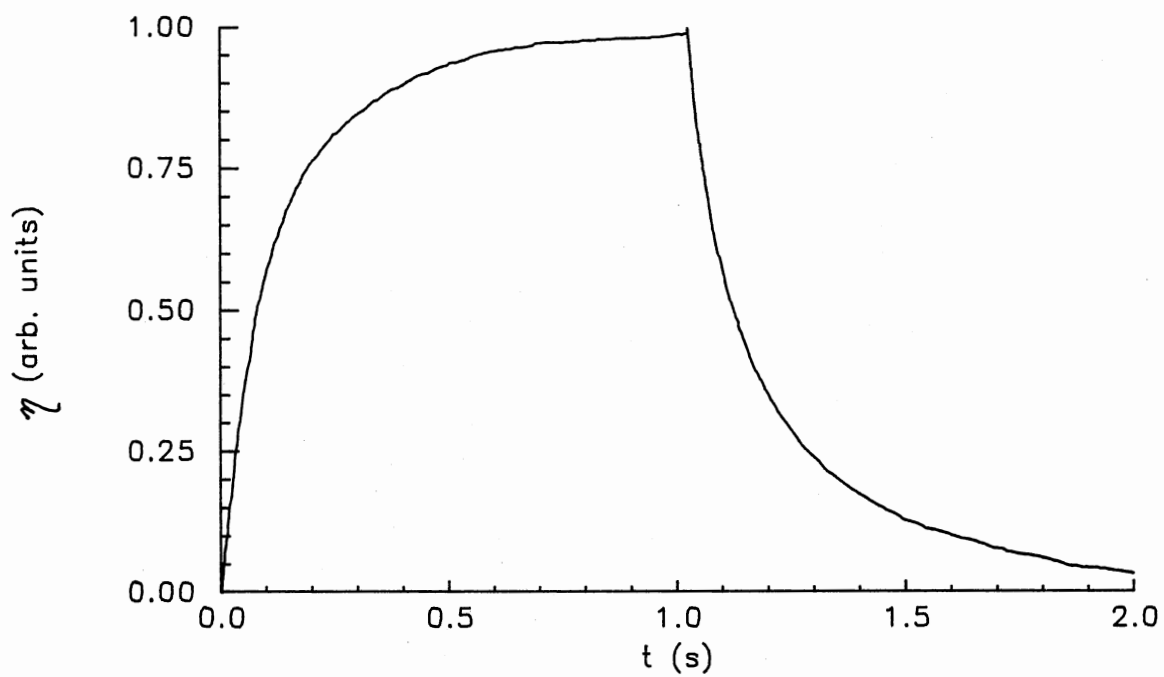erasure decay at 21°C

Figure 14. (continued) (c) dark decay at 125°C and
(d) erasure decay at 138°C
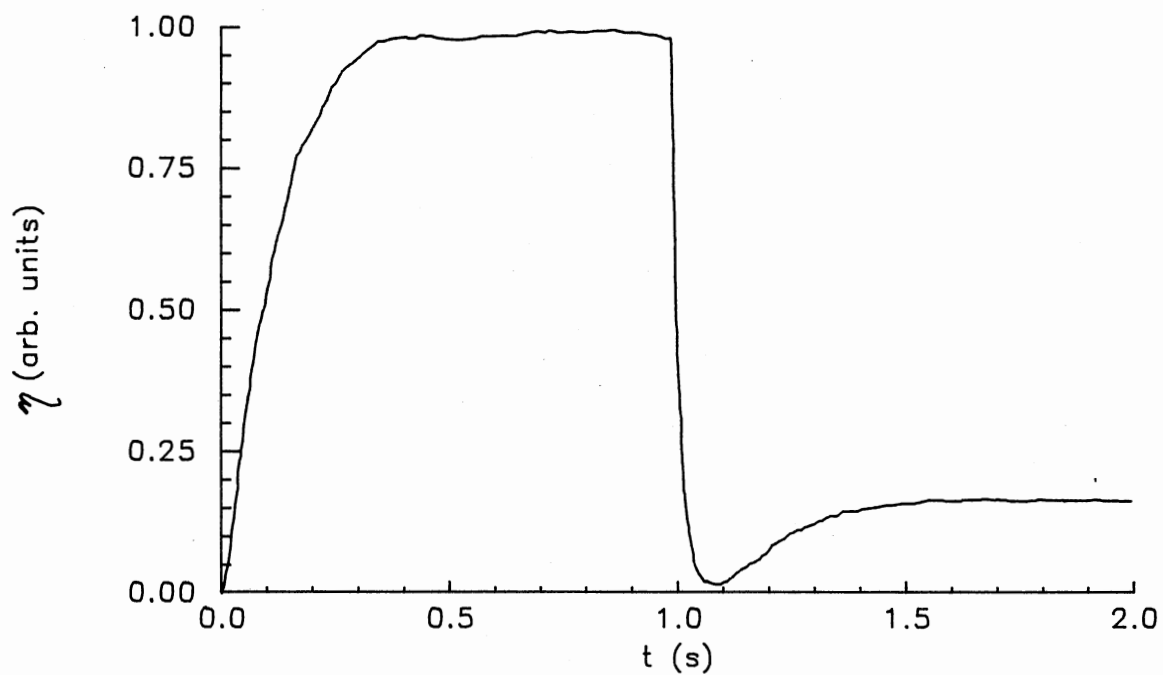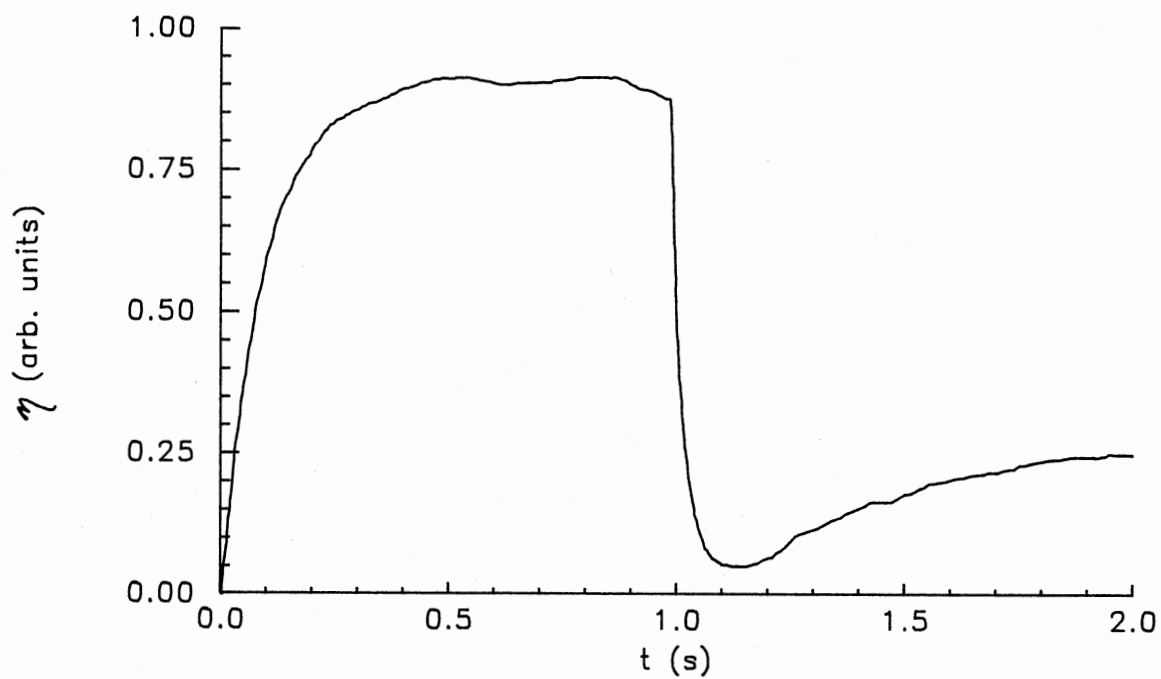
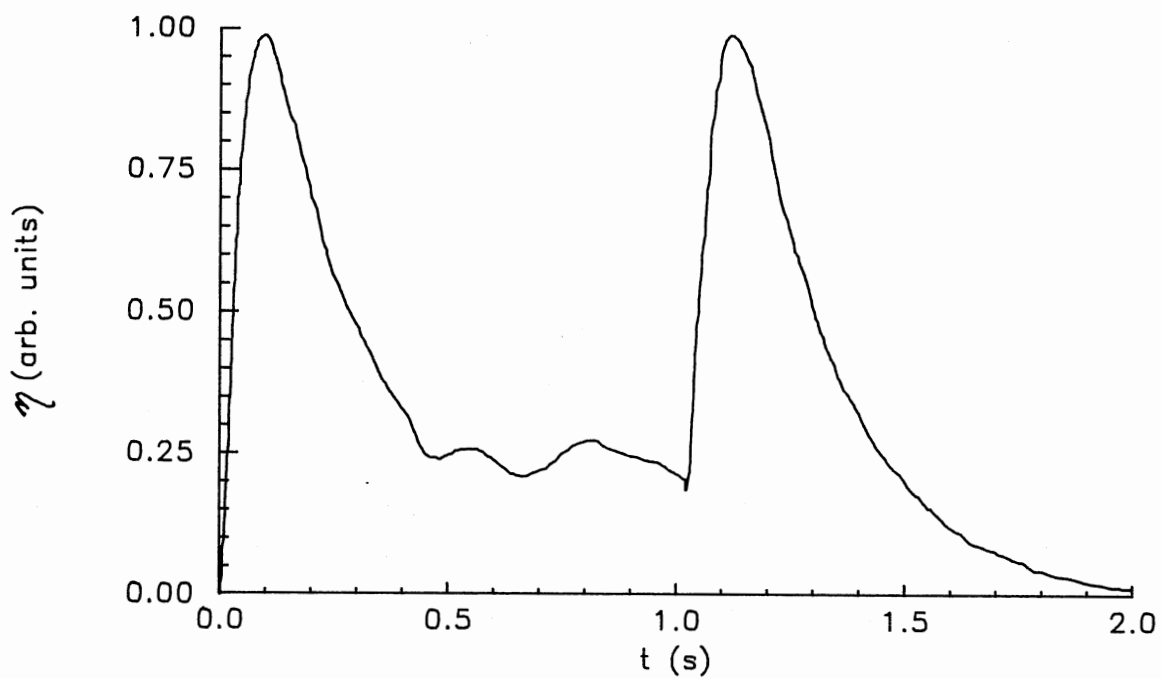Figure 14. (continued) (e) dark decay at 224°C and
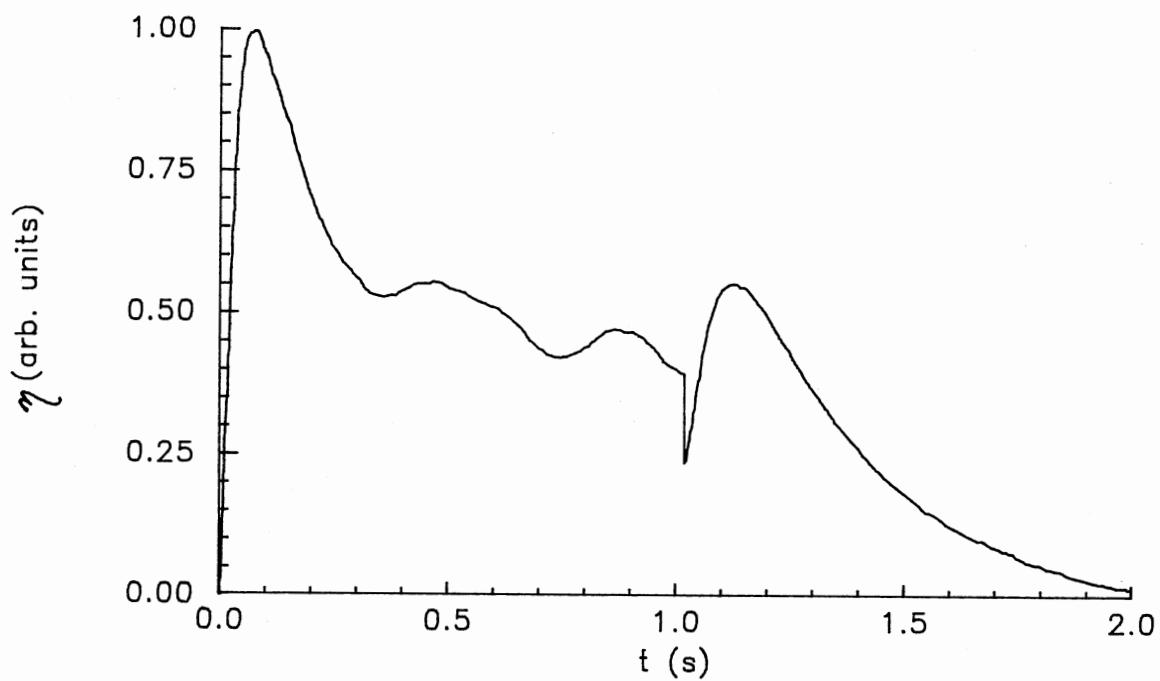(f) erasure decay at 231°C

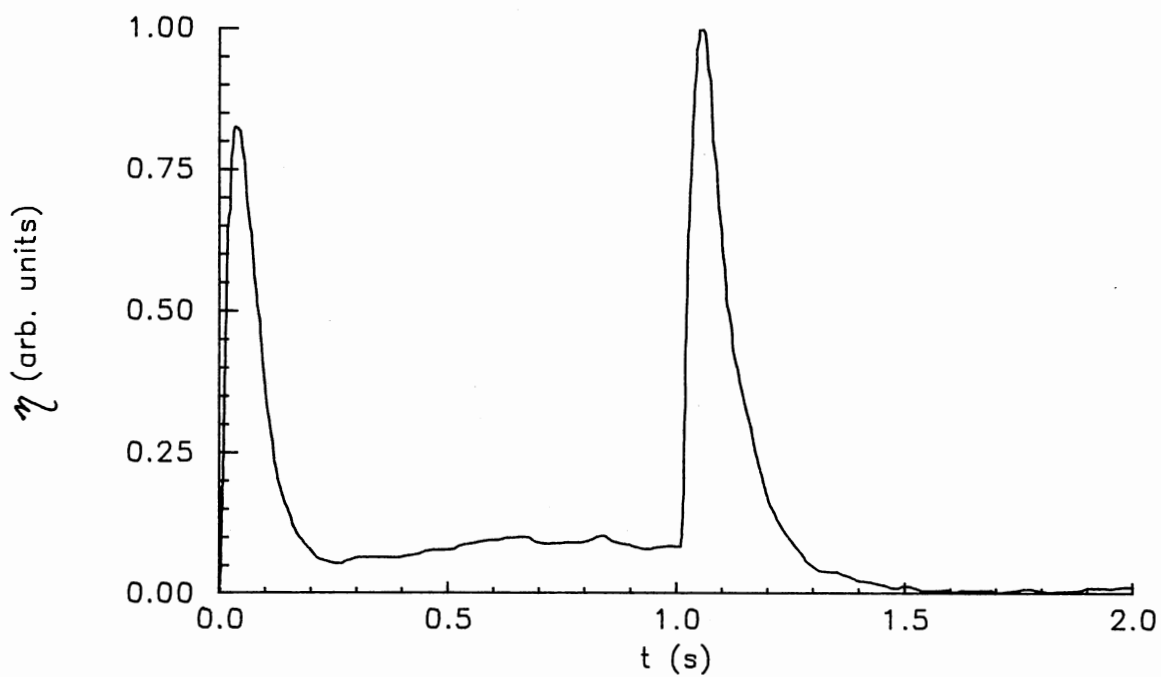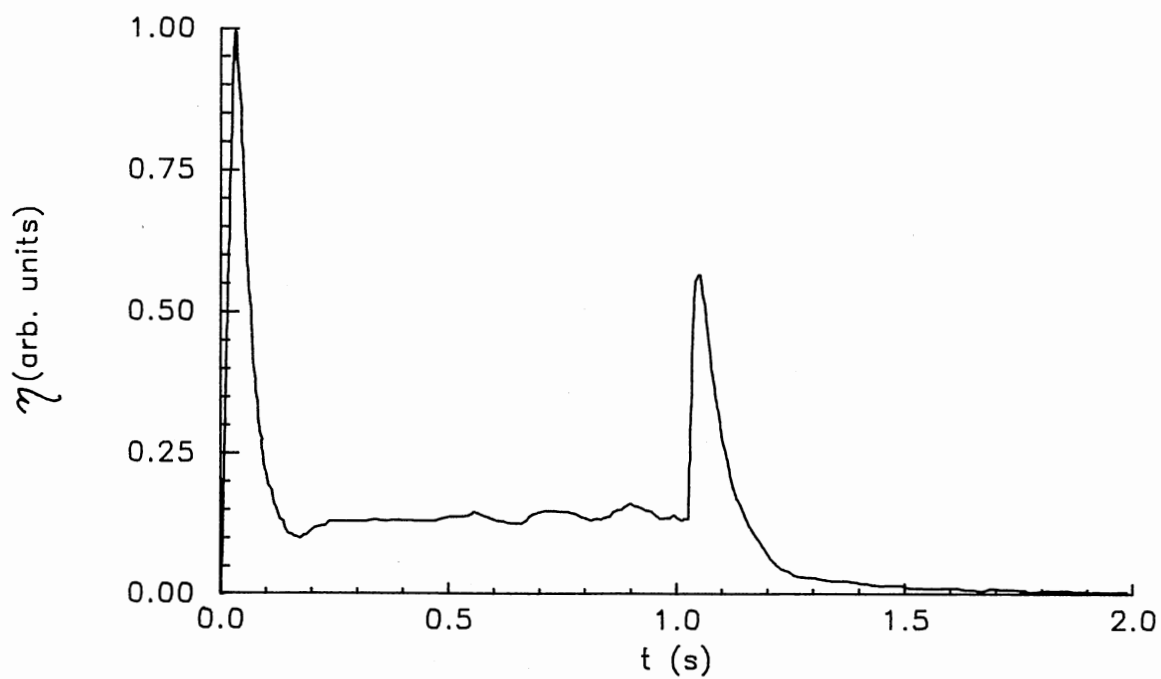Figure 14. (continued) (g) dark decay at 285°C and (h) erasure decay at 288°C

Figure 14. (continued)   (i) dark decay at 322°C and
(j) erasure decay at 316°C

develop which no longer resemble exponential behavior. In this region a maximum in the signal is reached after a short time in the writing cycle and a slower decay occurs. During the dark decay cycle, the signal then increases to another maximum before slowly decreasing to zero. Signal patterns for erasure decay are similar to those of dark decay but the secondary peak is slightly greater.

The band transport model of the PRE predicts a diffraction efficiency given by

$$\eta = A \sin^2(B[\exp(-t/\tau)\cos(\omega t)-1]-C\exp(-t/\tau)\sin(\omega t)) \quad (82)$$

during writing and

$$\eta = A \sin^2(\exp(-t/\tau) [B \cos(\omega t) + C \sin(\omega t)]) \quad (83)$$

during decay with the designations given earlier for A, B and C. Values for τ, the time constant during writing or decay, were obtained by fitting Equations (82) and (83) to the appropriate signal patterns.[12] Figure 15 shows the temperature dependence of τ acquired from the writing part of the PRE cycle. The value of τ increases approximately linearly between room temperature and 157°C. Above 157°C the rate parameter falls off rapidly with increasing temperature, and by 322°C it is reduced to about one-third of its maximum valve.

The PRE time constant is given by

$$\tau = \tau_{di} \frac{(1 + \tau_R/\tau_D)^2 + (\tau_R/\tau_E)^2}{[1 + \tau_R\tau_{di}/(\tau_D\tau_I)](1 + \tau_R/\tau_D) + (\tau_R/\tau_E)^2(\tau_{di}/\tau_I)} \quad .(71)$$

If the external field is set equal to zero and the time constants involved are replaced by their physical parameters
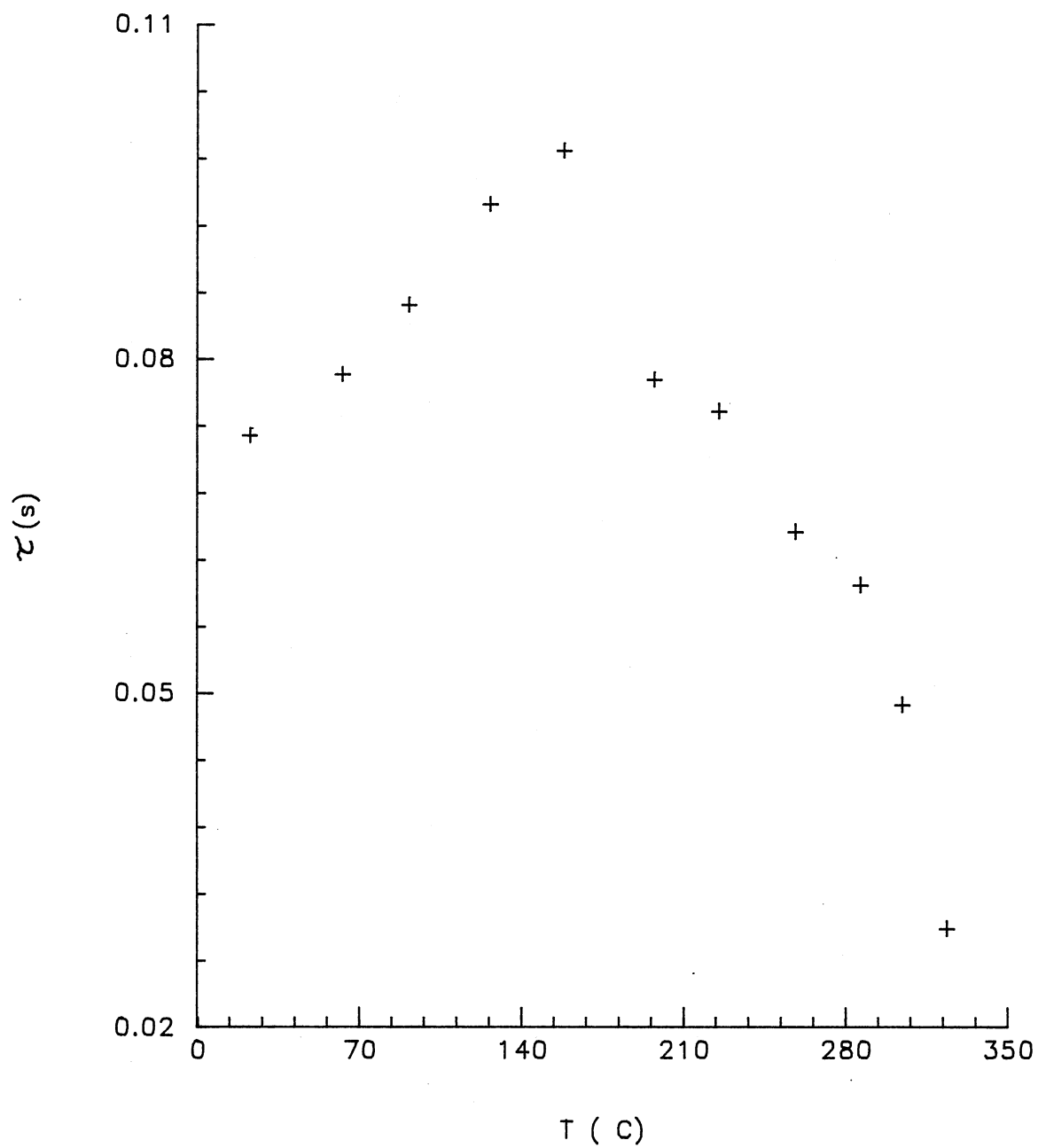
Figure 15. Time constant for the buildup of holographic
gratings in BSO as a function of temperature

from Equations (71) - (77), the decay constant can be expressed in terms of material and experimental parameters as;

$$\tau = [e\mu/(\sigma_T\gamma_R)] \frac{([\gamma_R N_A/\mu] + [k_B k_g^2 T/e])}{([4\pi e N_A/\varepsilon] + [k_B k_g^2 T/e])} \tag{84}$$

where $\sigma_T = \sigma_d + \sigma_p$ is the total conductivity which is the sum of the dark and photoconductivities, μ is the mobility, γ_R is the recombination rate coefficient, N_A is the number of acceptors, and k_g is the magnitude of the grating wavevector.

If the room-temperature values for the parameters given in Reference 23 are substituted into Equation (84), it is found that the first term in the denominator is approximately two orders of magnitude larger than the second term. The two terms in the numerator are of the same order of magnitude for BSO under the experimental conditions for this work. Thus, with this approximation, Equation (84) has an explicit temperature dependence which predicts a direct linear relationship between τ and T. This is the observed behavior for temperatures up to 157°C. Above this temperature τ decreases with increasing temperature. Therefore, one of the parameters in Equation (84) must have a strong enough temperature dependence to offset the explicit dependence on T above 157°C. Although several of these parameters can vary with temperature, it is expected that this offsetting temperature dependence of τ is dominated by the temperature variation of σ_T.

Dark conductivity increases exponentially with temperature when occupied traps exist below an energy band

and the mobility is relatively constant. It is reasonable to expect this in BSO over the temperature range in question.[37] To determine the importance of the dark conductivity contribution to the grating erasure, the decay of the signal when both writing beams were turned off was monitored as a function of temperature. Figure 16 shows the time constants obtained by fitting Equation (83) to the observed patterns. The dark decay time constant decreases about an order of magnitude between room temperature and 322°C, and shows none of the initial linear relationship exhibited by the writing time constant. The time constants of several temperatures (224, 257 and 285°C) were omitted since the model was unable to describe these signal patterns adequately. At these temperatures the patterns are undergoing a transition from simple rise-decay profiles to much more complex patterns. These "transition" curves are characterized by a very fast initial decay followed by a much slower buildup and subsequent decay. These curves also exhibit oscillatory patterns after the initial decay. These oscillations are probably connected to hole movement or absorption effects in the material and the theory does not account for them.

The dark decay time constant shows an approximately exponential decrease with increasing temperature. Combining this fact with the representative curves for dark and erasure decay would tend to suggest that the offsetting temperature dependent parameter is σ_d.
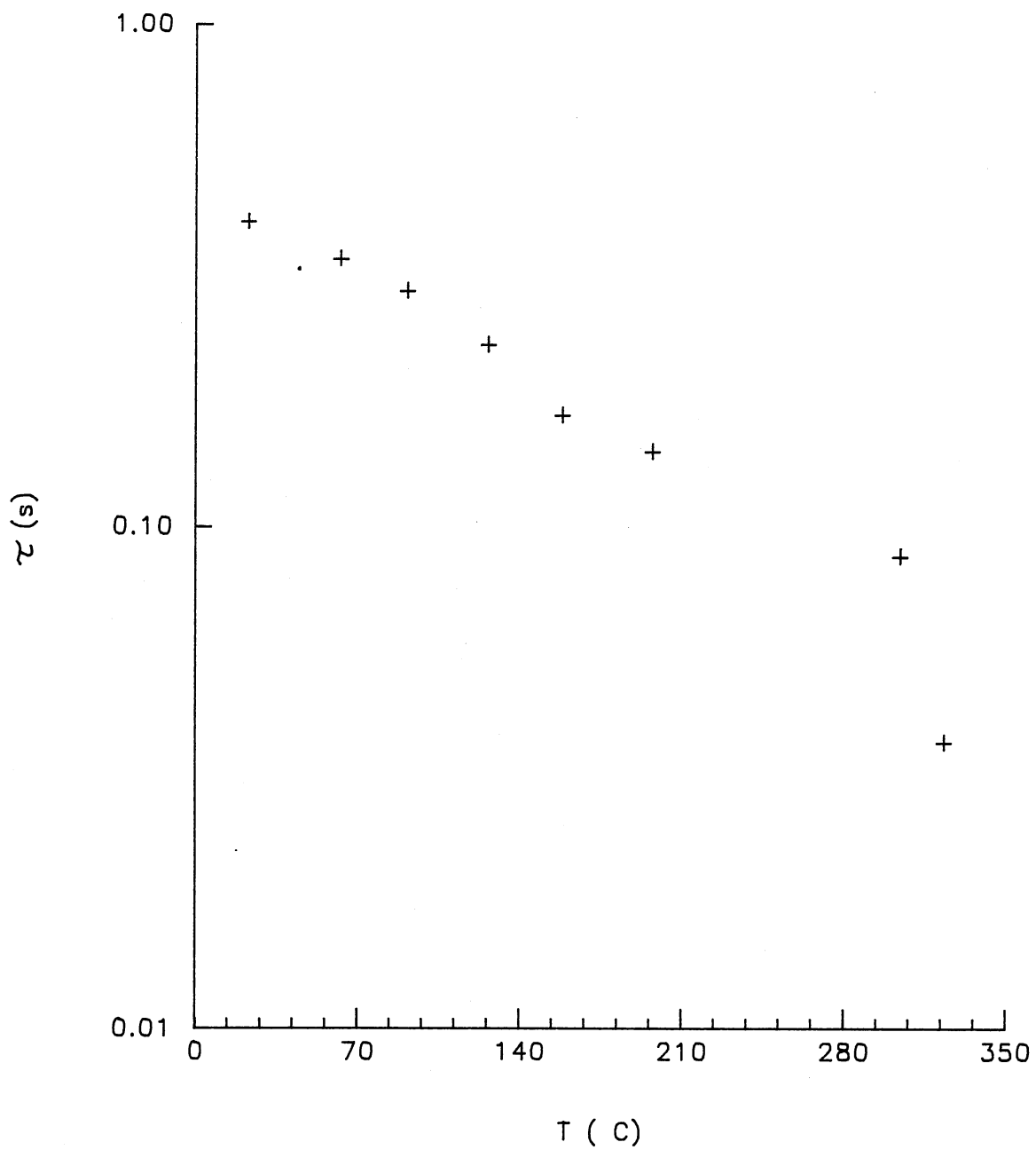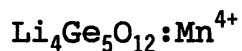
Figure 16. Dark decay times of holographic gratings in BSO
as a function of temperature

CHAPTER IV

FUTURE WORK

$$Li_4Ge_5O_{12}:Mn^{4+}$$

The results from Chapter II indicate the presence of two types of sites for the Mn^{4+} ions. One site undergoes radiationless quenching above 40 K and the other above 180 K. Although it is expected that these sites are the two types of Ge^{4+} sites in the crystal structure, it would be interesting to determine the symmetry of these sites and whether or not they are the Ge^{4+} sites. We were unable to determine the contribution to the scattering efficiency from absorption or dispersion. It would be useful to know which of these makes the dominant contribution. Finally, different forms of $Li_4Ge_5O_{12}:Mn^{4+}$ may not undergo the radiationless quenching that this form does at high temperatures. For most laser applications, room temperature activity is required. A different form may have a strong fluorescence at room temperature and would therefore be an interesting research area.

$$Bi_{12}SiO_{20}$$
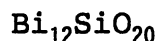
It is obvious from Chapter IV that the band transport model is inadequate in certain regions. The model cannot

describe the photorefractive dynamics at several temperatures and future work should focus on these "transition" temperatures to determine the physical process occurring at those temperatures. A useful study may concern the effect of the absorption on the photorefractive signal at higher temperatures. More work needs to be done to characterize the grating buildup and decay, and this could be accomplished through very fast pulses. If the laser beams writing the grating are chopped very quickly the nature of grating buildup and decay can be studied on a very fast time scale, and may give some insight into the validity of the band transport model.

REFERENCES CITED

1. S. Geschwind, P. Kisliuk, M.P. Klein, J.P. Remeika, and D.L. Wood, Phys. Rev. 126, 1684 (1962).

2. B. Henderson and T.P.P. Hall, Proc. Phys. Soc. 90, 511 (1967).

3. L.A. Riseberg and M.J. Weber, Solid State Commun. 9, 791 (1971).

4. J.F. Donegan, T.J. Glynn, G.F. Imbusch, and J.P. Remeika, J. Lumin. 36, 93 (1986).

5. A. Suchocki, J.D. Allen, R.C. Powell and G.M. Loiacono, Phys. Rev. B 36, 6729 (1987).

6. G.M. Loiacono and B.L. Greenberg (unpublished)

7. J.R. Salcedo, A.E. Siegman, D.D. Dlott, and M.D. Fayer, Phys. Rev. Lett. 41, 131 (1978).

8. A.M. Ghazzawi, J.K. Tyminski, R.C. Powell, and J.M. Walling, Phys. Rev. B 30, 7182 (1984).

9. H. Kogelnik, Bell Syst. Tech. J. 48, 2909 (1969).

10. J.J. Eichler, J. Eichler, J. Knof, and Ch. Noeck, Phys. Stat. Sol. (a) 52, 481 (1979).

11. D.J. Griffith, in "Introduction to Electrodynamics" (Prentice-Hall, Inc., Englewood Cliffs, 1981), p. 234

12. J.N. Demas, in "Excited State Lifetime Measurements" (Academic Press, New York, 1983).

13. F. Auzel, in "The Luminescence of Inorganic Solids", ed. B. DiBartolo (Plenum Press, New York, 1978), P. 67.

14. K.O. Hill, Appl. Opt. 10, 1695 (1971).

15. D.S. Hamilton, D. Heiman, J. Feinberg, and R.W. Hellwarth, Opt. Lett. 4, 124 (1979).

16. P.F. Liao, L.M. Humphrey, D.M. Bloomk, and S. Geschwind, Phys. Rev. B 20, 4145 (1979); P.F. Liao and D.M. Bloom, Opt. Lett. 3, 4 (1978).

17. H. Eichler, G. Salje, and H. Stahl, J. Appl. Phys. 44, 5383 (1973).

18. R.A. Mullen and R.W. Hellwarth, J. Appl. Phys. 58, 40 (1985)

19. S.I. Stepanov, V.V. Kulikov, and M.P. Petrov, Opt. Commun. 44, 19 (1982).

20. M.G. Miteva, IEEE J. Quantum Electron. QE-22, 1365 (1986).

21. G. Lesaux, G. Roosen, and A. Brun, Opt. Commun. 56, 374 (1986).

22. J.P. Herriau and J.P. Huignard, Ap[pl. Phys. Lett. 49, 1140 (1986).

23. G.C. Valley and M.B. Klein, Opt. Eng. 22, 704 (1983).

24. J.M. Jonathan, R.W. Hellwarth, and G. Roosen, IEEE J. Quantum Electron. QE-22, 1936 (1986).

25. M.A. Powell and C.R. Petts, Opt. Lett. 11, 36 (1986).

26. V.N. Astranov, A.V. Il'inskii, and M.B. Mel'nikov, Fiz. Tvard. Tella 28, 926 (1986) [Sov. Phys. Sol. State 28, 519 (1986)]

27. G. Pouliat, J.M. Cohen-Jonathan, M. Allain, J.C. Launay, and G. Roosen, Opt. Commun. 59, 266 (1986).

28. J.P. Huignard, H. Rajbenbach, Ph. Refregier, and L. Solymar, Opt. Eng. 24, 586 (1985).

29. L. Arizmendi and R.C. Powell, J. Appl. Phys. 62, 3. (1987).

30. N.V. Kukhtarev, V. Markov, S. Odulov, M. Soskin, and V. Vinetskii, Ferroelectrics 22, 949 (1977); 22, 961 (1977).

31. N.V. Kukhtarev, Pis'ma Zh. Tekh. Fiz. 2, 1114 (1976) [Sov. Tech. Phys. Lett. 2, 438 (1976)].

32. T.J. Hall, R. Javra, L.M. Connors and P.D. Foote, Prog. Quant. Electr. 10, FF. (1985).

33. A.M. Glass, Opt. Eng. 17, 470 (1978).

34. G.C. Valley, IEEE J. Quantum Electron, QE-19, 1637 (1983).

35. A. Marrakchi, R.V. Johnson, and A.R. Tanguary, Jr., J. Opt. Soc. America B $\underline{3}$, 321 (1986).

36. P. Gunter, Phys. Rep. $\underline{93}$, 199 (1982).

37. S.L. Hou, R.B. Lauer, and R.E. Aldrich, J. Appl. Phys. $\underline{44}$, 2652 (1973).

VITA

Jimmy Don Allen

Candidate for the Degree of

Master of Science

Thesis: OPTICAL SPECTROSCOPY IN $Li_4Ge_5O_{12}:Mn^{4+}$ AND THE PHOTOREFRACTIVE EFFECT IN $Bi_{12}SiO_{20}$

Major Field: Physics

Biographical:

Personal Data: Born in Altus, Oklahoma, January 2, 1961, the son of Donald and Sonja Allen.

Education: Graduated from the Kents Hill School, Kents Hill, Maine, in May, 1979; received Bachelor of Science degree with a double major in Engineering Physics and Mathematics in December, 1985 from Northeastern Oklahoma State University; completed requirements for the Master of Science degree at Oklahoma State University in December, 1988.

Professional Experience: Undergraduate Laboratory Instructor and tutor, Northeastern Oklahoma State University, August, 1984 to May, 1985; Undergraduate Research Assistant, Northeastern Oklahoma State University, May, 1985 to December, 1985; Graduate Lab Instructor, Oklahoma State University, January, 1986 to May, 1986; Graduate Research Assistant, Oklahoma State University, May, 1986 to present; Summer Intern, NASA-Langely Research Center, Summer 1987. Member of Sigma Pi Sigma honor society, the Society of Physics Students and the American Physical Society.